

The cosmology of ultralight scalar dark matter coupled to right-handed neutrinos

Ryan Plestid.^a Sophia Tevosyan^a

^aWalter Burke Institute for Theoretical Physics, California Institute of Technology, Pasadena, CA 91125, USA

E-mail: rplestid@caltech.edu, stevosya@caltech.edu

ABSTRACT: We consider ultralight scalar dark matter that couples to right-handed neutrinos. Due to the high density of neutrinos in the early universe, the background neutrino density dominates the dynamics of the scalar field, and qualitatively alters the field's cosmological evolution. This effect has not been included in previous literature, and changes the interpretation of cosmological data and its interplay with laboratory experiments. To illustrate these points a simplified model of a 1 + 1 setup with a single scalar field is analyzed.

We find that: *i*) The scalar field experiences an asymmetric potential and its energy density redshifts differently than ordinary matter. *ii*) Neutrino mass measurements at the CMB and oscillation experiments performed today complement one another (i.e., they constrain different regions of parameter space). *iii*) There exists potentially interesting cosmologies with either $O(1)$ variations in the dark matter density between the CMB and today, or $O(1)$ oscillations of neutrino mass.

Contents

1	Introduction	2
2	Zero crossings of the right-handed Majorana mass	3
2.1	Eigenvalues, masses, and states	4
2.2	Adiabatic approximation	6
2.3	Adiabatic transfer	7
3	Scalar field dynamics	7
3.1	The relic potential	8
3.2	Abundance of light scalars	9
4	Cosmological scenarios	9
4.1	Small amplitude initial conditions	10
4.2	Large negative amplitude initial conditions	10
4.3	Large positive amplitude initial conditions	16
4.4	Oscillations begin before neutrino decoupling	20
5	Phenomenology	22
5.1	Neutrino oscillation experiments	22
5.2	Neutrino mass and the CMB	23
5.3	Supernova cooling	26
5.4	Cosmologically stable condensate	27
5.5	Summary of constraints	30
6	Conclusions and outlook	32

1 Introduction

The identity of dark matter and the origin of neutrino masses are two of the most important outstanding questions in fundamental physics [1–3]. Most models that predict the origin of neutrino mass involve states that are singlets under the Standard Model gauge group (e.g., right-handed neutrinos) [1]; the same is true of many dark matter models [2, 3]. Since no gauge symmetry forbids their interaction, it is natural to consider couplings between dark matter and the progenitors of neutrino mass. In this paper we will be interested specifically in ultralight dark matter (ULDM with $m_\phi \ll 1$ eV), which acts as a classical field and whose oscillations can imprint observable signals in the neutrino sector.

Due to quantum statistics and simple phase space considerations, ULDM must have integer spin and obey Bose statistics [4, 5]. As a result, arguably the simplest model of ultralight dark matter (ULDM) is the oscillating homogeneous mode of a scalar field. This model of ULDM can easily accommodate the observed dark matter relic abundance via the so-called misalignment mechanism [6–9]. As already emphasized, assuming that the scalar field is a Standard Model gauge singlet, it will generically couple to the right-handed neutrino mentioned above. It is therefore natural, in this context, to consider the interplay between dark matter and neutrino phenomenology.

This simple observation has motivated a variety of studies involving neutrinos coupled to scalar fields [10–51]. This includes connections between mass-varying neutrinos and dark energy [10–16, 52] and neutrinos coupled to bosonic dark matter [17–29, 31–46]. In the present context, where the scalar field is a dark matter candidate, Refs. [17–25] have considered the potentially observable signals of so-called “distorted neutrino oscillations” (DiNOs) which may be observed in terrestrial experiments. These DiNOs arise from time-dependent neutrino masses which appear from expanding the see-saw like formula,

$$m_\nu \sim \frac{m_D^2}{m_N - g\phi(t)} \simeq \frac{m_D^2}{m_N} \left(1 + \frac{g\phi(t)}{m_N} + \dots \right), \quad (1.1)$$

where m_N is the bare Majorana mass, m_D is the Dirac mass, and g is the scalar right-handed neutrino coupling constant.

A common constraint that is discussed in the literature arises from the dynamics of ϕ in the early universe. If one assumes that the scalar field’s energy density red-shifts like matter, then at earlier epochs the field’s amplitude scales like $A_\phi \sim (1+z)^{3/2}$. If $gA_\phi(z)/m_N \sim O(1)$ at the epoch of the cosmic microwave background (CMB), then the sum of neutrino masses, $\sum m_\nu$, can be used to set constraints on the model [17–19].

Notice, however, that when $gA_\phi/m_N \sim O(1)$ the behavior of the system is very different than for $gA_\phi \ll m_N$. The left- and right-handed neutrinos will form a Dirac pair for $g\phi = m_N$, and transition from light, ν_L , to heavy, ν_H , states. This can induce decays $\nu_H \rightarrow \nu_L\phi$. Furthermore, if ϕ crosses a critical value $\phi_c = m_N/g$, then all the light neutrinos in the bath will become heavy, and this incurs an enormous energetic cost. As we will see in what follows, this energetic cost dominates the behavior of the scalar field’s potential in the early universe. This then substantially modifies the evolution of the scalar field, and the interpretation of constraints from $\sum m_\nu$ from the CMB.

The purpose of this paper is to study the dynamics of a scalar field coupled to right-handed neutrinos, properly accounting for the energy density of the background neutrino gas. This alters the scalar field's dynamics and depending on the initial conditions of the scalar field can lead to interesting phenomenology.

In what follows we will study a simplified model of neutrino scalar interactions. Our Lagrangian is defined by

$$\mathcal{L} = \mathcal{L}_{\text{SM}} + \frac{1}{2} \partial_\mu \phi \partial^\mu \phi + \bar{n}^c i \not{\partial} n^c - V_0(\phi) - (g\phi - m_N) n^c n^c - y L H n^c + \text{h.c.} , \quad (1.2)$$

where y is a Yukawa coupling, L is the left-handed lepton doublet, H is the Higgs doublet, n^c is a right-handed neutrino, ϕ is the scalar field, g the coupling constant, and $V_0(\phi)$ is the bare scalar potential. In what follows for simplicity, definiteness, and ease of comparison with other work, we will take

$$V_0(\phi) = \frac{1}{2} m_\phi^2 \phi^2 . \quad (1.3)$$

The scalar field ϕ is our dark matter candidate. When ϕ oscillates about the origin, m_ϕ is the mass of ULDM, and $m_\nu \sim m_D^2/m_N$ with $m_D = yv/\sqrt{2}$, and v the Higgs vacuum expectation value. We will assume that the physical scalar mass, m_ϕ , can assume very small values and do not consider naturalness issues related to the fine tuning of radiative corrections.

The rest of the paper is organized along the following lines. In Section 2 we discuss preliminaries that are necessary to understand the scalar field's dynamics. In Section 3 we discuss how the scalar field evolves throughout cosmic history. Next in Section 4 we consider various cosmological scenarios related to initial conditions and the temperature at which oscillations begin. In Section 5 we discuss a variety of constraints from cosmology, astrophysics, and laboratory experiments. Finally in Section 6 we summarize our findings and comment on potentially interesting future directions.

2 Zero crossings of the right-handed Majorana mass

In this section we will motivate why zero crossings (where the Majorana mass of n^c vanishes) appear when the dynamics of the scalar field are treated naively. This illustrates how and why the background potential from the neutrino gas must be included in the scalar dynamics.

To see why zero-crossings are generic when considering ULDM, let us work backwards from the present day assuming a standard misalignment mechanism. The (galactic) energy density of dark matter today is known and given by [53, 54]

$$\rho_{\text{DM,now}} \approx 9 \times 10^{-12} \text{ eV}^4 . \quad (2.1)$$

Assuming the scalar field ϕ oscillates about the origin, this fixes

$$A_\phi(z=0) = \frac{\sqrt{2\rho_{\text{DM,now}}}}{m_\phi} \approx 4 \times 10^{10} \text{ eV} \left(\frac{10^{-16} \text{ eV}}{m_\phi} \right) . \quad (2.2)$$

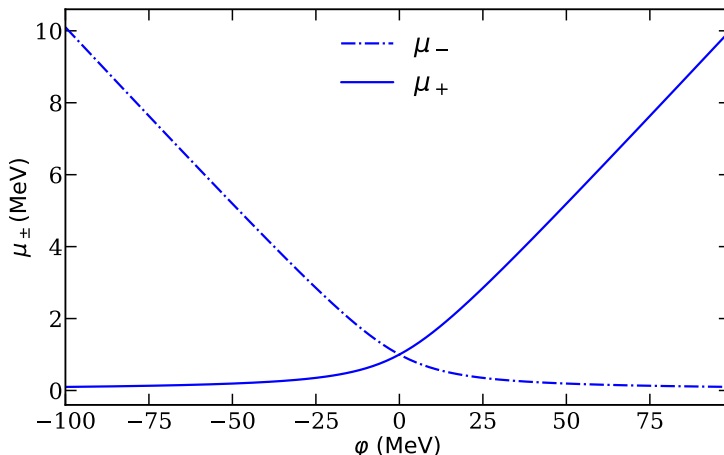


Figure 1: The absolute value of Eq. (2.5) (i.e., neutrino masses) for $m_D = 1$ MeV and $g = 0.1$. At the zero-crossing point $\varphi = 0$ we see that both eigenvalues are equal to m_D and the left- and right-handed neutrinos form a Dirac pair. For large positive φ , we see that μ_- approaches the seesaw limit, $m_D^2/(g\varphi)$, while μ_+ approaches $g\varphi$. The behavior is reversed for large negative φ . For large positive values of φ , $|\nu_- \rangle$ of Eq. (2.7) acts as the ‘light neutrino’ and $|\nu_+ \rangle$ of Eq. (2.6) as the ‘heavy neutrino’, and vice versa for large negative values of φ .

In the standard misalignment mechanism, the field begins to oscillate at a temperature T_{osc} defined by $3H(T_{\text{osc}}) = m_\phi$. Blue-shifting the field back to T_{osc} we find

$$A_\phi(z_{\text{osc}}) \sim \left(\frac{T_{\text{osc}}}{T_{\text{now}}}\right)^{3/2} A_\phi(z=0) \approx 3 \times 10^{24} \text{ eV} \left(\frac{0.65}{\gamma(T_{\text{osc}})}\right)^{3/4} \left(\frac{10^{-16} \text{ eV}}{m_\phi}\right)^{1/4}, \quad (2.3)$$

where $H = \gamma T^2/M_{\text{Pl}}$ with $M_{\text{Pl}} = 2.43 \times 10^{18}$ GeV the reduced Planck mass, and $\gamma^2 = \pi^2 g_*(T)/90$ with $g_*(T)$ the effective number of degrees of freedom. We take as $g_*(T) \approx 3.9$ for $T_{\text{osc}} \approx 0.1$ MeV. We see that even for rather small values of m_ϕ the amplitude of the field at the onset of oscillations is within three orders of magnitude of the Planck mass. It is therefore very difficult, without considering very small values of g , to avoid $A_\phi \simeq m_N/g$.

As we will see in what follows, the dynamics of the system at large energy densities are not properly accounted for by simply re-scaling $A_\phi \sim (1+z)^3$. To understand these features we first turn to the eigenvalues of the neutrino mass matrix, then discuss the adiabatic approximation, and the adiabatic transfer of neutrino species. We return to the scalar field’s dynamics in Section 3.

2.1 Eigenvalues, masses, and states

Let us consider the neutrino mass matrix at a fixed field value ϕ ,

$$M = \begin{pmatrix} 0 & m_D \\ m_D & g\phi - m_N \end{pmatrix} = \begin{pmatrix} 0 & m_D \\ m_D & g\varphi \end{pmatrix}, \quad (2.4)$$

with $m_D = yv/\sqrt{2}$. In the second equality we have introduced $\varphi = \phi - \phi_c$ where $\phi_c = m_N/g$. The absolute values of the eigenvalues of Eq. (2.4) are

$$\mu_{\pm} = \frac{1}{2} \left(\sqrt{4m_D^2 + (g\varphi)^2} \pm g\varphi \right) , \quad (2.5)$$

and the normalized eigenvectors in terms of the flavor basis (ν, n^c) are

$$|\nu_+\rangle = \sin\theta |\nu\rangle + \cos\theta |n^c\rangle , \quad (2.6)$$

$$|\nu_-\rangle = \cos\theta |\nu\rangle - \sin\theta |n^c\rangle , \quad (2.7)$$

where

$$\sin^2\theta = \frac{\mu_-}{\sqrt{4m_D^2 + (g\varphi)^2}} . \quad (2.8)$$

The coupling to scalar-quanta in the mass basis is given by

$$\mathcal{L}_{\text{int}} = (\sin^2\theta \nu_+ \nu_+ + \cos^2\theta \nu_- \nu_- + 2\sin\theta \cos\theta \nu_- \nu_+) \varphi . \quad (2.9)$$

There are both on- and off-diagonal couplings.

Notice that for large and positive φ , the eigenvalues approach the approximate (see-saw) values

$$\begin{aligned} \mu_+ &\approx g\varphi , \\ \mu_- &\approx \frac{m_D^2}{g\varphi} , \end{aligned} \quad (2.10)$$

while (again for $\varphi \gg m_D/g$) the eigenvectors become

$$|\nu_+\rangle \approx |n^c\rangle + \frac{m_D}{g\varphi} |\nu\rangle , \quad (2.11)$$

$$|\nu_-\rangle \approx |\nu\rangle - \frac{m_D}{g\varphi} |n^c\rangle . \quad (2.12)$$

We see that ν_+ is the ‘heavy’ mass eigenstate that is mostly composed of the sterile neutrino, while ν_- is the ‘light’ mass eigenstate mostly composed of the active neutrino. The roles are reversed for large and negative $\varphi \ll -m_D/g$, where we find that

$$\begin{aligned} \mu_+ &\approx \frac{m_D^2}{g\varphi} , \\ \mu_- &\approx g\varphi , \end{aligned} \quad (2.13)$$

with eigenvectors

$$\begin{aligned} |\nu_+\rangle &\approx |\nu\rangle + \frac{m_D}{g\varphi} |n^c\rangle , \\ |\nu_-\rangle &\approx -|n^c\rangle + \frac{m_D}{g\varphi} |\nu\rangle . \end{aligned} \quad (2.14)$$

For $\varphi = 0$ the masses are degenerate, with ν_{\pm} forming a Dirac-pair with mass $|\mu_{\pm}| = m_D$. In Fig. 1 we plot the masses of the two eigenstates (absolute value of the eigenvalues) as a function of φ .

When considering cosmology or particle kinematics (e.g., for a decay) it is convenient to track which neutrino species is heavy and which is light. We therefore introduce ν_L and ν_H . For example, ν_L is defined by (cf. Fig. 1)

$$|\nu_L\rangle = \begin{cases} |\nu_+\rangle & \phi < \phi_c \\ |\nu_-\rangle & \phi > \phi_c . \end{cases} \quad (2.15)$$

It is similarly useful to introduce the mixing angle $\sin\theta_L$

$$\sin\theta_L = \langle \nu_L | n^c \rangle = \begin{cases} \cos\theta & \phi < \phi_c \\ \sin\theta & \phi > \phi_c , \end{cases} \quad (2.16)$$

such that $\sin^2\theta_L \leq 1/2$.

2.2 Adiabatic approximation

Let us next consider the equations of motion for the fields ν and n^c . It is convenient to assemble them into a vector $N = (\nu, n^c)^T$. Then the equations of motion read,

$$[i\partial \cdot \bar{\sigma} - \underline{M}(t)]N = 0 . \quad (2.17)$$

All underlined matrices act in flavor space (as opposed to $\bar{\sigma}^\mu$ which acts on spinor indices). These equations may be conveniently re-cast in the instantaneous eigenbasis by diagonalizing $\underline{M}(t)$ at each instant in time. Let us introduce the rotation matrix

$$\underline{R} = \begin{pmatrix} \cos\theta(t) & \sin\theta(t) \\ -\sin\theta(t) & \cos\theta(t) \end{pmatrix} . \quad (2.18)$$

Inserting $\underline{R}^T(t)\underline{R}(t)$ into Eq. (2.17), and acting from the left with $\underline{R}(t)$ we obtain

$$[i\partial \cdot \bar{\sigma} \underline{1} - \underline{\mathcal{M}}(t) + i\underline{R}(t)\partial_t\underline{R}^T(t)]\mathcal{N} = 0 , \quad (2.19)$$

where $\mathcal{N} = (\nu_+, \nu_-)^T$ are the instantaneous mass eigenstates and $\underline{\mathcal{M}}(t) = \text{diag}[\mu_+(t), \mu_-(t)]$. With some elementary trigonometric identities, one can show that $i\underline{R}(t)\partial_t\underline{R}^T(t) = (\partial_t\theta)\sigma_2$ with $\sigma_2 = \begin{pmatrix} 0 & -i \\ i & 0 \end{pmatrix}$. We then obtain

$$\left[i\partial \cdot \bar{\sigma} \underline{1} - \underline{\mathcal{M}}(t) + \dot{\theta}(t)\sigma_2 \right] \mathcal{N} = 0 . \quad (2.20)$$

In the limit of slowly varying $\theta(t)$, we may drop the third term in Eq. (2.20). This is the adiabatic approximation and gives,

$$[i\partial \cdot \bar{\sigma} \underline{1} - \underline{\mathcal{M}}(t)]\mathcal{N} = 0 . \quad (2.21)$$

The adiabatic approximation is valid when [55, 56]

$$m_D^2 \gg g\dot{\phi} , \quad (2.22)$$

which physically corresponds to the gap in the spectrum, $\Delta \sim m_D$, being larger than the rate of change of the Majorana mass $\frac{d}{dt}(m_N - g\phi)$. Whenever Eq. (2.22) is satisfied jumps between the two instantaneous eigenstates are exponentially suppressed.

As an aside, since the Majorana mass of n^c crosses zero, it is interesting to ask if non-perturbative particle production can take place; we find that it does not. This issue has been extensively studied in the context of inflation [57–60] and for a single fermion particle production generically occurs whenever a particle’s mass vanishes. This is because around this limit, the gap between positive and negative energy solutions (to the Klein-Gordan, Dirac, or other relativistic wave equation) vanishes. In the present context the off-diagonal Dirac mass supplies a non-zero gap even for a vanishing Majorana mass. It is easily checked that whenever Eq. (2.22) is satisfied non-perturbative particle production is exponentially suppressed. We therefore conclude that for the dynamics of interest the adiabatic approximation is valid, there is no particle production, and the n_+ and n_- populations are conserved. This conservation is only violated by heavy neutrino decays $\nu_H \rightarrow \nu_L + \phi$.

2.3 Adiabatic transfer

In the adiabatic approximation the populations of each instantaneous eigenstate (i.e., the labels \pm) are separately conserved. Therefore, if $\phi(t)$ crosses ϕ_c (or equivalently if φ crosses 0), then light-neutrinos will become heavy. This gives a non-thermal mechanism for the generation of heavy neutrinos from a thermal or relic population of light neutrinos. The heavy neutrino can then decay into the light neutrino and scalar, producing a population of relativistic light neutrinos

$$\nu_H \rightarrow \nu_L + \phi , \quad (2.23)$$

where ν_H is the heavier instantaneous eigenstate at a given time.

The decay rate in the rest frame for $\nu_H \rightarrow \nu_L + \phi$ is given by

$$\Gamma = \frac{g^2 \cos^2 \theta \sin^2 \theta}{16\pi} \left(\frac{m_H^4 - m_L^4}{m_H^3} \right) . \quad (2.24)$$

where

$$\sin^2 \theta \cos^2 \theta = \frac{m_D^2}{(g\varphi)^2 + 4m_D^2} . \quad (2.25)$$

The mass of the heavy and light states are also functions of the scalar field. In the limit where $g\varphi \ll 2m_D$ we find,

$$\Gamma \simeq \frac{g^4}{8\pi} |\varphi| \left(1 + O\left(\frac{g\varphi}{m_D} \right) \right) . \quad (2.26)$$

Decays are almost instantaneous on cosmological timescales. This results in most decays occurring near the mass degenerate limit, and very little energy being released.

3 Scalar field dynamics

Having established how the fermion masses change with ϕ , we now turn to the equations of motion for ϕ

$$\ddot{\phi} + 3H\dot{\phi} + V'(\phi, t) = 0 . \quad (3.1)$$

Here, $V(\phi, t)$ contains two contributions,

$$V(\phi, t) = V_0(\phi) + V_\nu(\phi, T) , \quad (3.2)$$

where $V_\nu(\phi, T)$ is the energy density of neutrinos whose mass depends on ϕ .

The form of $V_\nu(\phi, T)$ depends on whether or not neutrinos are in thermal equilibrium with the Standard Model bath. Above the temperature of neutrino decoupling $T \geq T_{\nu, \text{dec}} \approx 1$ MeV, light mostly-active neutrinos are in thermal equilibrium and dynamically adjust their phase space distribution in response to changes to their mass.¹ Below $T_{\nu, \text{dec}}$ neutrinos are a relic species, and are essentially inert. In this limit the neutrino number density is conserved. We now discuss the relic and thermal potentials separately.

3.1 The relic potential

After neutrino decoupling, the momentum distribution of neutrinos is fixed, and (assuming a standard cosmology for neutrino decoupling) is described by a massless Fermi-Dirac distribution with $T \simeq T_{\nu, \text{dec}}$. As the universe expands, the momentum distribution redshifts and the number distribution scales as (see [10, 12, 61] for a discussion in the context of mass-varying neutrinos)

$$n(k, T) = n_F \left(k \frac{T_{\nu, \text{dec}}}{T}, T_{\nu, \text{dec}} \right) = \frac{1}{e^{k/T} + 1} , \quad (3.3)$$

with an integrated number density that scales as $(T/T_{\nu, \text{dec}})^3$ as the universe cools. This phase space distribution then contributes to a ‘‘relic potential’’. Changing the mass of all neutrinos shifts the energy density by

$$\mathcal{E}(\phi) - \mathcal{E}(\phi = 0) = \frac{1}{2} m_\phi^2 \phi^2 + \int \frac{d^3 k}{(2\pi)^3} n_\pm(k) \left(\sqrt{k^2 + \mu_\pm^2} - \sqrt{k^2 + \mu_\pm^2(\phi = 0)} \right) . \quad (3.4)$$

If we assume an arbitrary number density of + and – states then the relic potential is given by

$$V_{\text{relic}}(T) = \int \frac{d^3 k}{(2\pi)^3} n_{\mu_-}(k, T) \sqrt{k^2 + \mu_-^2} + \int \frac{d^3 k}{(2\pi)^3} n_{\mu_+}(k, T) \sqrt{k^2 + \mu_+^2} . \quad (3.5)$$

In the limit of a single relic species (\pm) with a number density given by Eq. (3.3), the resulting effective potential simplifies in the limit of $T \gg \mu_\pm$ and $T \ll \mu_\pm$. These two limiting forms are given by

$$V_{\text{relic}} \simeq \begin{cases} \frac{3\zeta(3)}{4\pi^2} T^3 \mu_\pm(\phi) & T \ll \mu_\pm \\ \frac{1}{48} T^2 \mu_\pm^2(\phi) & T \gg \mu_\pm . \end{cases} \quad (3.6)$$

¹As we discuss in Section 4.4, even above $T_{\nu, \text{dec}}$ neutrino interactions rates are sometimes too slow to maintain thermal equilibrium.

3.2 Abundance of light scalars

The scalars we consider are light, and could be produced thermally via $\bar{\nu}_L \nu_L \rightarrow \phi\phi$ in the early universe. The thermally averaged cross section (assuming $m_L \ll T$) is dominated by heavy neutrino exchange (see Section 5.3) and is given parametrically by

$$\Gamma = \langle \sigma n v \rangle \sim \frac{T^3}{m_H^2} \left(\frac{m_L}{m_H} \right)^2. \quad (3.7)$$

Setting this rate equal to Hubble in radiation domination we find the decoupling temperature T_* ,

$$\frac{T_*^2}{M_{\text{Pl}}} \sim \frac{T_*^3}{m_H^2} \left(\frac{m_L}{m_H} \right)^2 \implies T_* \sim \frac{m_H^4}{M_{\text{Pl}} m_L^2}. \quad (3.8)$$

Taking $m_L \leq m_\nu \sim 0.1$ eV this gives,

$$T_* \gtrsim 40 \text{ GeV} \times \left(\frac{m_H}{1 \text{ GeV}} \right)^4. \quad (3.9)$$

At this epoch m_H will be dominated by $|g\varphi_{0,\text{est}}|$. As we will see in what follows, (specifically see Eq. (4.5)) this then guarantees that at T_* the relic density of ϕ particles that have frozen out will be negligible at BBN. We therefore do not consider the thermal population of scalars in the rest of our analysis.

4 Cosmological scenarios

The presence of background potentials that are proportional to the neutrino density can dramatically alter the scalar field dynamics. The precise cosmological history depends qualitatively on the the initial conditions, and the ordering of various time scales. Specifically we will be interested in the value of the field's initial condition, ϕ_0 , relative to the critical field value ϕ_c . In this section we describe how the cosmological history is modified.

The mass of the scalar field determines at what temperature oscillations onset. This always occurs during radiation domination such that $H = \gamma T^2/M_{\text{Pl}}$ with $\gamma = \sqrt{\pi^2 g_*(T)}/90$. Solving for $3H = m_\phi$ then gives,

$$T_{\text{osc}} = \sqrt{\frac{m_\phi M_{\text{Pl}}}{3\gamma(T_{\text{osc}})}} \approx 4 \times 10^5 \text{ eV} \left(\frac{0.65}{\gamma(T_{\text{osc}})} \right)^{1/2} \left(\frac{m_\phi}{10^{-16} \text{ eV}} \right)^{1/2}, \quad (4.1)$$

where we have benchmarked the number of effective degrees of freedom using $g_*(T_{\text{osc}}) = 3.91$. For $m_\phi \lesssim 10^{-14}$ eV, we have $T_{\text{osc}} \lesssim T_{\nu,\text{dec}}$ and can therefore use the relic potential for the entirety of the scalar field's dynamics. We discuss the case of $m_\phi \gtrsim 10^{-14}$ eV in Section 4.4. For $m_\phi \lesssim 10^{-14}$ eV the analysis of the next two sections applies immediately. For heavier scalars, our constraints on parameter space may be viewed as conservative, since any acceptable cosmology will eventually lead to a relic neutrino population at $T < T_{\nu,\text{dec}}$. We discuss the dynamics of the scalar field during epochs where neutrinos are in thermal equilibrium qualitatively in Section 4.4.

4.1 Small amplitude initial conditions

For large- m_N or small- g the value of ϕ_c can be so large that a standard misalignment mechanism is valid from T_{osc} until today. This scenario is simple to analyze, and its domain of validity can be easily inferred by blue-shifting the present-day dark matter density to T_{osc} .

By assumption (in order to have “small” initial conditions) we require $|\phi_0| \leq \phi_c$. The potential is well approximated as quadratic, and the amplitude will red-shift in time like $A_\phi \sim (T/T_{\text{osc}})^{3/2}$. The relic density today is given roughly by

$$\rho_{\text{DM,now}} = \frac{1}{2} m_\phi^2 \phi_0^2 \left(\frac{T_{\text{now}}}{T_{\text{osc}}} \right)^3 . \quad (4.2)$$

Demanding that ϕ_0 in Eq. (4.2) is less than ϕ_c gives an upper-bound on the relic density as a function of m_ϕ , m_N , and g . Therefore, using $\rho_{\text{DM,now}} = 9 \times 10^{-12} \text{ eV}^4$, in order for $|\phi_0| \leq \phi_c$ can be written as

$$m_N \gtrsim 3 \times 10^{14} \text{ GeV} \left(\frac{10^{-16} \text{ eV}}{m_\phi} \right)^{1/4} \left(\frac{g}{0.1} \right) . \quad (4.3)$$

This limit leads to very heavy right-handed neutrinos, which will therefore be Boltzmann suppressed and out of the bath well before BBN. Notice, also, that the Majorana mass of the right-handed neutrino is so large that even for $g \sim O(1)$ there will be no observable DiNO signatures [17, 18].

4.2 Large negative amplitude initial conditions

For lighter right-handed neutrinos the inequality Eq. (4.3) will be violated and the Majorana neutrino mass will naively cross zero. In reality, at early epochs the neutrino density is so large that the relic potential can cause the $\phi = \phi_c$ region to become kinematically forbidden. During the epoch following neutrino decoupling, our potential is given by

$$V(\phi, t) = V_0(\phi) + V_{\text{relic}}(\phi, T) , \quad (4.4)$$

with $V_0(\phi)$ given by Eq. (1.3) and V_{relic} given by Eq. (3.6), with $\mu = \mu_+$ since according to Eq. (2.13) this is the light eigenstate for large negative values of ϕ . We take the heavy eigenstate to be Boltzmann-suppressed, assuming that at early times (when the field is stuck by Hubble friction) that the Majorana mass, $|m_N - g\phi_0|$, is large compared to the temperature.

Absence of Zero Crossings

We begin by estimating initial conditions assuming (naively) that the energy density in the scalar field oscillations red-shifts like matter $\rho \sim T^3$. We will revisit this assumption below. Without loss of generality² we can assume the field begins at $\phi_0 < 0$. We then estimate

²If the field begins at $0 < \phi_* < \phi_c$ then it will “drop” much earlier than $T \sim \sqrt{m_\phi M_{\text{pl}}}$, and then get stuck by Hubble friction at its turning point at $\phi_0 < 0$.

the initial conditions using the density of dark matter today $\rho_{\text{DM,now}} \approx 9 \times 10^{-12} \text{ eV}^4$, and the relation,

$$\phi_{0,\text{est}} = \sqrt{\frac{2\rho_{\text{DM,now}}}{m_\phi^2}} \left(\frac{T_{\text{osc}}}{T_{\text{now}}} \right)^{3/2} \approx 3 \times 10^{24} \text{ eV} \left(\frac{m_\phi}{10^{-16} \text{ eV}} \right)^{1/4}, \quad (4.5)$$

where $T_{\text{now}} = 2.3 \times 10^{-4} \text{ eV}$. The initial field value is very large at T_{osc} as is the initial neutrino density. For such a large initial field value the potential is well-approximated by the bare potential, and we neglect the relic potential in the calculation of Eq. (4.5). The left-turning point, ϕ_L , is initially equal to ϕ_0 , but will decrease as the universe cools due to the red-shifting of the field's energy density.

Zero crossings will occur if the right turning point crosses ϕ_c . However, we find that the inequality $\phi_R < \phi_c$ is satisfied for all temperatures. In what follows we will assume that $m_D \gg T$ such that the low-temperature approximation to the relic potential is valid for ϕ close to ϕ_c .³ At early times, when ϕ_R is closest to ϕ_c , the right-turning point is given by

$$\phi_R \simeq \phi_c - \frac{2m_D}{g} \left(\frac{m_D^2 n_\nu^2 - \rho_{\text{DM}}^2}{2m_D n_\nu \rho_{\text{DM}}} \right) \simeq \phi_c - \frac{2m_D}{g} \left(\frac{m_D n_\nu}{m_\phi^2 \phi_L^2} \right). \quad (4.6)$$

In deriving Eq. (4.6), we used the fact that ϕ_R is close to ϕ_c and that ϕ_L is very large and negative. Therefore, to compute ϕ_R we may set the energy density equal to the relic potential (neglecting the bare contribution), whereas for ϕ_L we set the energy density equal to the bare potential (neglecting the relic contribution).

Equation (4.6) implies that zero crossings do not occur with initial conditions to the left of ϕ_c for the highest temperatures. Notice that the term in parentheses is independent of T for $n_\nu \sim T^3$ and $\phi_L^2 \sim T^3$. Therefore, in this high temperature regime, the right-turning point is also independent of temperature, and the field does not cross ϕ_c during its dynamical evolution. At lower temperatures, the field does not even approach ϕ_c and we conclude that zero crossings occur at no temperatures.

A possible exception to our analysis occurs when $m_D \ll T$, in which case the pre-factor of the relic potential scales as T^2 as opposed to the $\rho_{\text{DM}} \sim T^3$ growth of the scalar field's energy density. This may then allow the energy density in the scalar field to overcome the potential barrier from the relic potential. We comment briefly on this possibility in Section 6.

Modified Redshifting of the Dark Matter Energy Density

Since the potential is highly anharmonic, the field will (generically) not red-shift like matter. Nevertheless, as we will now argue, over most of cosmic history the $\rho \sim T^3$ scaling is a very good approximation. There is a short epoch where the field loses energy density faster than standard dark matter, but this period of time is short and leads to an $O(1)$ change in the dark matter energy density, after which the field resumes its behavior scaling as

³At sufficiently large $|\phi - \phi_c|$ one can always have $m_L \ll T$, such that the high temperature expansion of the relic potential must be used at large field values.

$\rho \sim T^3$. This $O(1)$ change can spoil concordance between estimates/measurements of the dark matter energy density at different cosmological epochs.

The Hubble damping of a scalar field in a generic potential can be obtained by computing the time-averaged ratio of $\dot{\phi}^2$ relative to ρ [9],

$$\gamma(\rho) = \frac{\langle \dot{\phi}^2 \rangle}{\rho} = 2 \frac{\int_{\chi_L}^{\chi_{\min}} (1 - \frac{V}{V_{\max}})^{1/2} d\chi + \int_{\chi_{\min}}^{\chi_R} (1 - \frac{V}{V_{\max}})^{1/2} d\chi}{\int_{\chi_L}^{\chi_{\min}} (1 - \frac{V}{V_{\max}})^{-1/2} d\chi + \int_{\chi_{\min}}^{\chi_R} (1 - \frac{V}{V_{\max}})^{-1/2} d\chi}, \quad (4.7)$$

where we re-scale the field $\psi = g\phi/(2m_D)$, and introduce

$$\chi = \psi - \psi_c = \frac{g}{2m_D}(\phi - \phi_c). \quad (4.8)$$

The turning points, $\chi_{L,R}$ are a function of ρ . Assuming rapid oscillations (relative to Hubble) the time-averaged energy density obeys the non-linear differential equation

$$\frac{d\rho}{dt} = -3H\gamma(\rho)\rho, \quad (4.9)$$

which can be solved given a solution $\gamma(\rho)$. To determine how χ_{\min} and the turning points $\chi_{L,R}$ change over time, we will investigate the evolution of the shape of the potential and the oscillations of the scalar field with temperature. The shape of the potential is characterized by two dimensionless ratios

$$\kappa = \frac{g^2 n}{4m_\phi^2 m_D}, \quad (4.10)$$

$$\psi_c = \frac{g\phi_c}{2m_D}. \quad (4.11)$$

In terms of these variables, the potential is given by

$$V(\chi) = \begin{cases} \frac{4m_D^2 m_\phi^2}{g^2} \left(\frac{1}{2}(\chi + \psi_c)^2 + \kappa\lambda_+ \right) & T \ll m_D\lambda_+ \\ \frac{4m_D^2 m_\phi^2}{g^2} \left(\frac{1}{2}(\chi + \psi_c)^2 + \frac{m_D T^2}{48n} \kappa\lambda_+^2 \right) & T \gg m_D\lambda_+ \end{cases}, \quad (4.12)$$

where

$$\lambda_\pm = \chi \pm \sqrt{\chi^2 + 1}. \quad (4.13)$$

Notice that $\kappa \propto n \propto T^3$ is largest at high temperatures. When κ is large the minimum of the potential is pushed to large negative field values, which leads to a light neutrino mass $m_L \ll m_D$. At very high temperatures, where the relativistic approximation in Eq. (3.6) and Eq. (4.12) applies, the minimum scales as $\chi_{\min} \sim (\kappa m_D/T)^{1/4} \sim T^{1/2}$. As the temperature decreases, χ_{\min} shifts towards the origin, and m_L increases until $m_L(\chi_{\min}) \gg T$. At this point the non-relativistic approximation to Eq. (3.6) and Eq. (4.12) is appropriate, and the potential is globally well approximated by

$$V(\chi) \simeq \frac{1}{2}(\chi + \psi_c)^2 - \frac{\kappa}{2\chi} \quad \text{for } \kappa, \psi_c \gg 1, \quad (4.14)$$

whose minimum occurs at⁴

$$\chi_{\min} \simeq \frac{1}{3} \left(\frac{1}{2^{2/3}} (\sqrt{27\kappa(27\kappa + 8\psi_c^3)} - 27\kappa - 4\psi_c^3)^{1/3} + \frac{2^{2/3}\psi_c^2}{(\sqrt{27\kappa(27\kappa + 8\psi_c^3)} - 27\kappa - 4\psi_c^3)^{1/3}} - \psi_c \right). \quad (4.15)$$

One can clearly see by inspection that there are three different qualitative regimes: $\kappa^{1/3} \gg \psi_c$, $\kappa^{1/3} \sim \psi_c$, and $\kappa^{1/3} \ll \psi_c$. For example, when $\kappa^{1/3} \gg \psi_c$ the minimum scales $\chi_{\min} \simeq -(\kappa/2)^{1/3}$, when $\kappa^{1/3} \sim \psi_c$ Eq. (4.15) must be used, and when $\kappa^{1/3} \ll \psi_c$ then $\chi_{\min} \simeq -\psi_c$.

These different scalings lead to different shapes of the potential. In Fig. 2 we show the different shapes that one encounters as the universe cools. The plots are shown at different “magnifications”, which are set by the amplitude of oscillations,

$$A_L = |\chi_L - \chi_{\min}|. \quad (4.16)$$

As shown in Fig. 2a, at early times $A_L \gg \kappa^{1/3} \gg \psi_c$ and the potential looks like a harmonic oscillator with a steep barrier near $\chi \sim O(1) \ll A_L$. Since $|\chi_{\min}| \ll A_L$, the barrier and the minimum occur at roughly the same location. As the universe cools, A_L drops like $T^{3/2}$ (with some corrections which we discuss below), and eventually A_L becomes comparable to χ_{\min} when $A_L \gtrsim \psi_c \gtrsim \kappa^{1/3}$. During this epoch the shape of the potential resembles a harmonic oscillator centered near $\chi_{\min} \simeq -\psi_c$. The steep barrier near $\chi \sim O(1)$ is well separated (in units of A_L) from the minimum. Finally, Hubble friction causes the amplitude to become sufficiently small that the steep barrier is energetically inaccessible (i.e., very far away in units of A_L), and the dynamics are well approximated by the bare potential.

We now return to the red-shifting of the dark matter energy density and Eq. (4.7). In the early stages of the universe (Fig. 2a), the amplitude of the field is very large compared to the minimum of the potential $\chi_L \gg \chi_R \simeq \chi_{\min}$. As a result, the first integral (i.e., the “left” portion of the oscillation) in both the numerator and denominator of Eq. (4.7) provide the dominant contributions. The minimum of the potential is very close to $\chi = 0$ (i.e., $\chi_{\min}/\chi_L \ll 1$), and we can think of the potential as a harmonic oscillator with a “brick wall” at $\chi = 0$. Since the reflected dynamics on the half-interval $[\chi_L, 0]$ are equivalent to the dynamics that would occur in a symmetric oscillator centered at $\chi = 0$, we find $\gamma = 1 + O(\chi_{\min}/\chi_L)$ and the field red-shifts like matter.

As shown in Fig. 2b, the left-turning point χ_L decreases due to Hubble friction as the universe cools. In this epoch $A_L \sim \psi_c \sim \kappa^{1/3}$ and the left-amplitude, $A_L = |\chi_L - \chi_{\min}|$, becomes comparable to the right-amplitude, $A_R = |\chi_R - \chi_{\min}|$. Both the left- and right-oscillations provide $O(1)$ contributions to the integrals in Eq. (4.7). In this regime, the “brick wall” is now offset from the minimum of the potential which has shifted to $\chi_{\min} \simeq -\psi_c$. Now, when the fields bounces off the wall at $\chi = 0$, it does so in the right-portion of its oscillation, which increases the average kinetic energy ($\langle \dot{\phi}^2 \rangle$) per oscillation cycle. This

⁴This result is derived by taking Eq. (4.14), counting $\chi_{\min} \sim \kappa^{1/3} \sim \psi_c \sim \lambda$, and expanding in the $\lambda \rightarrow \infty$ limit.

leads to a short epoch where $\gamma \gtrsim 1$ (cf. Eq. (4.17)). Consequently, there is a sudden decrease in the scalar field’s energy density relative to the naive expectation of $\rho \propto (T/T_{\text{osc}})^3$ during this epoch.

Eventually, as shown in Fig. 2c, this epoch ends when $A_R \sim A_L \ll \psi_c \sim \chi_{\text{min}}$. At this point the steep barrier from the relic potential becomes energetically inaccessible, and the field oscillates in its symmetric bare potential about the minimum. In this epoch $\gamma = 1$, and the scalar field’s energy density again red-shifts like matter.

To compute the drop in the scalar field’s energy density (relative to the typical scaling with matter) during the epoch depicted in Fig. 2b we solve Eq. (4.9). It is convenient to model the relic potential as a “brick wall” as alluded to above. This amounts to a reflective boundary condition at $\chi = 0$ in addition to the bare scalar potential. Within this approximation, Eq. (4.7) may be re-written as (using $y = (\chi - \chi_{\text{min}})/A_L$)

$$\begin{aligned} \gamma_{\text{BW}}(c) &\equiv 2 \frac{\int_0^1 (1-y^2)^{1/2} dy + \int_0^c (1-y^2)^{1/2} dy}{\int_0^1 (1-y^2)^{-1/2} dy + \int_0^c (1-y^2)^{-1/2} dy} \\ &= \frac{\frac{\pi}{2} + c\sqrt{1-c^2} - 2 \cot^{-1}\left(\frac{c+1}{\sqrt{1-c^2}}\right)}{\frac{\pi}{2} + \sin^{-1}(c)}, \end{aligned} \quad (4.17)$$

where $c \equiv \chi_{\text{min}}/A_L$. The above equation applies for $0 \leq c \leq 1$, whereas for $c \geq 1$,

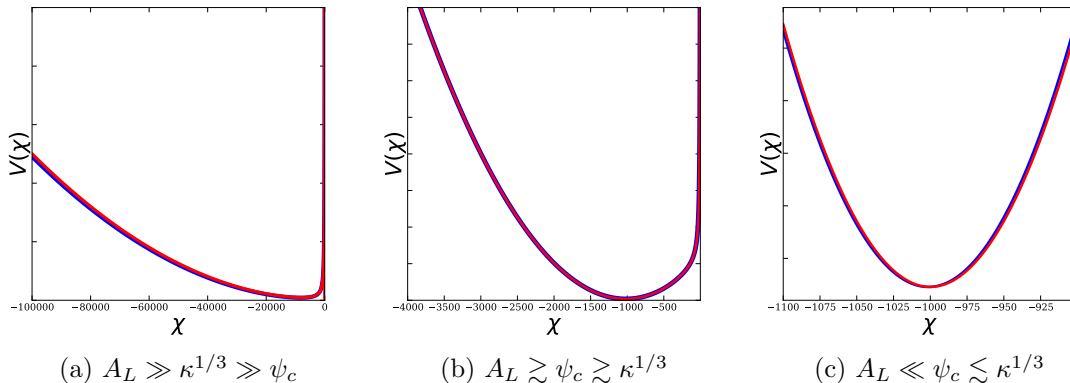


Figure 2: Different shapes of the (dimensionless) potential throughout cosmic history for $\chi_0 < 0$ and $\psi_c = 10^3$. Note the different scales on the abscissa (x -axis) between (a)-(c), which are representative of A_L . The full potential is plotted in blue, and the approximation from Eq. (4.14) is plotted in red. (a) Initial conditions are such that the left turning-point is large $\chi_L \gg \chi_{\text{min}}$. The scalar field is reflected at the origin and spends almost all of its time in a harmonic potential. (b) Hubble friction reduces the amplitude of oscillations until it is comparable to χ_{min} . At this stage the steep “brick wall” barrier causes the field to have a larger average kinetic energy than it otherwise would in a symmetric harmonic potential. (c) Eventually the amplitude becomes sufficiently small that the right turning-point is far removed from the “brick wall” and the field oscillates in a symmetric harmonic potential.

corresponding to the case where the wall is energetically inaccessible, we have $\gamma_{\text{BW}}(c) = 1$. The relationship between c and the energy density ρ is given by,

$$c = \frac{\chi_{\text{min}}}{\chi_L} \simeq \frac{m_\phi \phi_c}{\sqrt{2\rho}} = \frac{m_\phi m_N}{g\sqrt{2\rho}}. \quad (4.18)$$

Notice that $\gamma(c=0) = 1$, which corresponds to the epoch shown in Fig. 2a where the brick wall occurs at (or very close to) χ_{min} .

To obtain the shift in the energy density away from the naive $\rho \sim T^3$ scaling expected for non-relativistic matter, we may compute

$$\Delta(\rho) = \int_\rho^{\rho_0} \left[\frac{1}{\gamma(\rho')} - 1 \right] d \log(\rho'), \quad (4.19)$$

which leads to

$$\left(\frac{\rho}{\rho_0} \right) e^{\Delta(\rho)} = \left(\frac{T}{T_{\text{now}}} \right)^3. \quad (4.20)$$

Using the brick wall model and Eq. (4.18) to change variables from ρ' to c' , we find that

$$\Delta_{\text{BW}}(c) = -2 \int_{c_0}^c \left[\frac{1}{\gamma_{\text{BW}}(c')} - 1 \right] d \log(c'), \quad (4.21)$$

and integrating numerically we find $\Delta_{\text{BW}}(c \geq 1) \approx 0.693$, which leads to a decrease of $e^{-\Delta_{\text{BW}}} \approx 0.5$. Therefore, the net result of the asymmetric potential generated by the neutrino background is a dark matter energy density which experiences a sudden drop by $\sim 50\%$ relative to what would be obtained for a cosmic history where $\gamma = 1$.

The temperature at which this large drop in the dark matter energy density occurs can be estimated (using $A_L \sim |\chi_{\text{min}}| \sim \psi_c$ as is appropriate for the epoch depicted in Fig. 2b) by equating $\phi_{0,\text{est}} \left(\frac{T}{T_{\text{osc}}} \right)^{3/2} = \phi_c$, which gives

$$\frac{T_{\text{drop}}}{T_{\text{now}}} = \left(\frac{m_\phi \phi_c}{\sqrt{2\rho_{\text{DM,now}}}} \right)^{2/3} = 0.4 \times \left(\frac{m_N}{1 \text{ GeV}} \right)^{2/3} \left(\frac{m_\phi}{10^{-16} \text{ eV}} \right)^{2/3} \left(\frac{0.1}{g} \right)^{2/3}. \quad (4.22)$$

For $T_{\text{now}} < T_{\text{drop}} \lesssim T_{\text{CMB}}$, i.e. when Fig. 2c corresponds to the current epoch, we expect that this will (badly) spoil concordance between CMB measurements and estimates of the dark matter relic abundance today. While this parameter space is naively ruled out, our results motivate a detailed study of transient equations of state as we discuss in more detail in Section 6.

By way of contrast, if $T_{\text{drop}} < T_{\text{now}}$, i.e. when Fig. 2a corresponds to the current epoch, then the amplitude of oscillations are still large enough that the $O(1)$ effect has not occurred. However this then has consequences for present day measurements of neutrino mass which will vary rapidly as a function of time due to the large oscillations in this regime. Specifically, we expect $O(1)$ modifications to time-averaged neutrino oscillation parameters, such that existing constraints from DiNOs (sensitive to $\sim 5\%$ distortions [17, 18]) entirely rule out this region of parameter space.

4.3 Large positive amplitude initial conditions

Next, let us consider initial conditions in which $\phi_0 > \phi_c$. Unlike the case when $\phi_0 < 0$, where the relic potential only served to modify the (effectively conservative) scalar field's dynamics, in this case the heavy- and light-neutrino eigenstates can exchange roles at some point in cosmic history. We will take $\phi_0 \gg \phi_c$ such that ν_H is Boltzmann suppressed, and our potential again has the form

$$V(\phi, T) = V_0(\phi) + V_{\text{relic}}(\phi, T) , \quad (4.23)$$

with $\mu = \mu_-$ since according to Eq. (2.10) this is the light eigenstate for large positive values of ϕ . We will mostly be concerned with the epoch at CMB and those following it, so we take $T \ll m_D \lambda_-$ and our potential in terms of χ and ψ_c has the form

$$V(\chi) = \frac{4m_D^2 m_\phi^2}{g^2} \left(\frac{1}{2}(\chi + \psi_c)^2 + \kappa \lambda_- \right) , \quad (4.24)$$

with λ_- once again given by Eq. (4.13).

The minimum of the potential is found by solving $V' = 0$, or equivalently

$$\frac{\psi_c}{\kappa} + \left(1 - \frac{\chi_{\text{min}}}{\sqrt{\chi_{\text{min}}^2 + 1}} \right) = -\frac{\chi_{\text{min}}}{\kappa} . \quad (4.25)$$

Clearly the behavior of the solution is controlled by the ratio

$$r = \frac{\psi_c}{\kappa} . \quad (4.26)$$

When $\kappa \gg 1/r^{3/2}$ (or equivalently $\kappa \ll \psi_c^3$), the location of the minimum is given by

$$\chi_{\text{min}} \simeq \left(\frac{1-r}{\sqrt{r(2-r)}} \right) . \quad (4.27)$$

This formula is most useful when $r \sim O(1)$.

At high temperatures, $r \rightarrow 0$, and the minimum moves to large field values. It is convenient to expand $\lambda_- \simeq 1/(2\chi)$ in Eq. (4.24), and solve for the minimum. Doing so one finds,

$$\chi_{\text{min}} \simeq \frac{1}{3} \left[\frac{\kappa R}{\sqrt[3]{\frac{1}{4}\kappa^2 (3(\sqrt{81-24R}+9) - 4R) R}} - \sqrt[3]{\kappa R} + \sqrt[3]{\frac{1}{4}\kappa (3(\sqrt{81-24R}+9) - 4R)} \right] , \quad (4.28)$$

where

$$R = r^3 \kappa^2 = \frac{\psi_c^3}{\kappa} , \quad (4.29)$$

and the expression in the square brackets is $\sim O(1/R^{1/6})$ as $R \rightarrow \infty$. The minimum therefore scales as $\kappa^{1/3}/R^{1/6} \sim \kappa^{1/6}$ at high temperatures.

As we will see in what follows, the cosmology of a field trapped at $\chi \geq 0$ is much more dramatic than for a field whose initial conditions are taken to be $\chi < 0$. For this reason, the red-shift dependence of the energy density is less interesting, and we instead focus on a different phenomenon in which the identity of neutrinos in the bath changes character.

Zero-crossings and overclosing the universe

As the universe cools r increases, and is eventually $\sim O(1)$. Notice that for $r \sim O(1)$ the minimum of the potential, Eq. (4.27), occurs close to $\chi = 0$ and for $r \geq 1$ actually occurs at negative values of χ . During this epoch the field will generically cross $\chi = 0$. This has dramatic consequences for the subsequent cosmology.

As χ crosses 0, all of the neutrinos in the bath adiabatically convert from light-eigenstates to heavy-eigenstates. There is then a short period of rapid decays (see Section 2.3). This can be summarized as,

$$\nu_{-,L} \xrightarrow{\text{adiabatic}} \nu_{-,H} \xrightarrow{\text{decay}} \phi + \nu_{+,L} , \quad (4.30)$$

where we have tracked both “heavy” and “light”, as well as the adiabatically conserved labels “−” and “+”. This essentially instantaneously converts the ν_- population into a ν_+ population, which effectively “flips” the relic potential such that it no longer opposes the bare potential and the minimum now occurs at $\phi \approx 0$ or equivalently $\chi \approx -\psi_c$ (see Fig. 3b). The field is now misaligned from the new minimum with a large initial amplitude; oscillations begin immediately, and the energy density stored in the coherent oscillations of the field can overclose the universe.

Since the density of neutrinos is a monotonically decreasing function of temperature, so too is the χ_{\min} of Eq. (4.27), and there will always exist a temperature T_{cross} such that zero-crossings occur. We numerically solve for the m_N where $T_{\text{cross}} = T_{\text{now}}$ by determining when the left-turning point χ_L crosses zero, where χ_L satisfies the condition

$$V(\chi_L) - V(\chi_{\min}) = \rho_{\text{DM,now}} , \quad (4.31)$$

with χ_{\min} given by Eq. (4.27) and Eq. (4.28) in the appropriate regimes.⁵ We find that over most of parameter space, the zero-crossing point is very well-approximated by simply taking the value of m_N for which the minimum of the potential crosses zero, and dividing it by 200. The temperature for which the minimum crosses zero is easily determined by setting the $r = 1$ (*cf.* Eq. (4.27)), which yields

$$m_{N_{\text{cross,now}}} \approx \frac{1}{200} \frac{g^2(3\zeta(3)/4\pi^2)T_{\text{now}}^3}{2m_\phi^2} . \quad (4.32)$$

However, for small enough values of m_N , the minimum of the potential becomes so close to zero that the zero-crossing point becomes essentially independent of m_N , and this approximation breaks down (see Fig. 8). We find that when $m_\phi \gtrsim 10^{-13}$ eV for $g = 10^{-4}$ or $m_\phi \gtrsim 10^{-10}$ eV for $g = 0.1$, the field will always cross zero before today.

⁵Where we use Eq. (4.40) to determine m_D in terms of m_N , m_ϕ , and g .

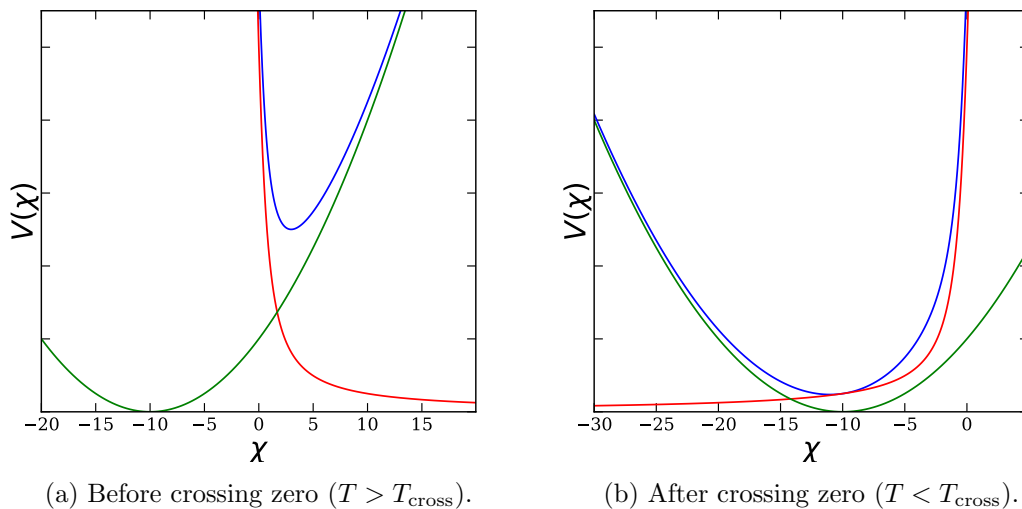


Figure 3: Different shapes of the (dimensionless) potential throughout cosmic history for $\chi_0 > 0$. The full potential Eq. (4.24) is plotted in blue, the relic potential is plotted in red, and the bare (harmonic) potential is plotted in green. **(a)** Before zero crossings, the relic potential serves as a steep “wall” that points in the opposite direction of the bare potential. This leads to small oscillations “in the cup” created by the two potentials. **(b)** After crossing zero, the relic potential “flips” and now drives χ towards large negative values. The net result is large oscillations centered around the minimum of the bare potential $\chi \sim -\psi_c$ (or $\phi \sim 0$).

If $T_{\text{cross}} > T_{\text{now}}$, then zero crossings have certainly occurred in our cosmic history which implies that Majorana masses satisfying (see Fig. 8)

$$m_N \gtrsim 3 \times 10^6 \text{ GeV} \left(\frac{g}{0.1} \right)^2 \left(\frac{10^{-16} \text{ eV}}{m_\phi} \right)^2, \quad (4.33)$$

lead to cosmologies where the field passes through $\chi = 0$ at some point in its evolution.

After zero crossings occur, the potential has the shape shown in Fig. 3b. Near the minimum at $\phi = 0$, the potential is nearly zero, $V(\phi) \approx 0$, since the bare potential vanishes and neutrinos are nearly massless. The energy density stored in the field is therefore given by the value of the potential at zero-crossing, or

$$\rho_{\text{DM,cross}} = V_{\text{cross}} = V_0(\phi_c) + V_{\text{relic}}(\phi_c) = \frac{1}{2} m_\phi^2 \phi_c^2 + m_D n_\nu. \quad (4.34)$$

The oscillations are approximately harmonic, and we can assume a typical scaling of dark matter energy density with temperature $\rho_{\text{DM,now}} \sim \left(\frac{T_{\text{now}}}{T_{\text{cross}}} \right)^3$. To avoid exceeding today’s dark matter energy density, we therefore demand that

$$\left[\frac{1}{2} m_\phi^2 \phi_c^2 + m_D n_\nu \right] \times \left(\frac{T_{\text{now}}}{T_{\text{cross}}} \right)^3 \leq \rho_{\text{DM,now}}. \quad (4.35)$$

Which leads to the condition

$$m_N \lesssim 600 \text{ eV} , \quad (4.36)$$

where we use⁶ Eq. (4.27) to calculate T_{cross}^3 by setting $r = 1$ and replacing m_N with $200m_N$ based on the discussion surrounding Eq. (4.32)

$$T_{\text{cross}}^3 = \frac{400m_\phi^2 m_N}{g^2(3\zeta(3)/4\pi^2)} . \quad (4.37)$$

Using the typical see-saw relationship $m_N \sim m_D^2/m_\nu$ one can see that $T_{\text{cross}}^3 \sim \left(\frac{m_\phi^2}{m_D m_\nu}\right) m_D^3$ such that $T_{\text{cross}} \ll m_D$ and the use of the low-temperature expansion of the relic potential is justified. At sufficiently high temperatures $T_{\text{cross}} \gg m_D$ one must switch to the high-temperature expansion of the relic potential which could lead to zero crossings at earlier times. This possibility is discussed in Section 6.

In summary, if

$$m_N \lesssim \max\left(\text{Eq. (4.33)}, \text{Eq. (4.36)}\right) . \quad (4.38)$$

then the scalar field's energy density does not overclose the universe.

Modified Seesaw Relationship

For cosmologies in which $T_{\text{cross}} < T_{\text{now}}$, the typical see-saw relationship does not hold in the present epoch i.e., $m_{\nu,\text{now}} \neq m_D^2/m_N$. This is because if $T_{\text{cross}} < T_{\text{now}}$ then the present day scalar's potential resembles Fig. 3a. The effective Majorana mass is therefore given by $m_N^{\text{eff}}(t) = |g\phi(t) - m_N| = g\varphi(t)$ (cf. Eq. (2.4)) and this can differ substantially from m_N even after time averaging.

We find that $m_D^2/|g\varphi_{\text{min}}|$ provides a reasonable parametric estimate for the time-averaged value of the neutrino mass $\langle m_\nu \rangle_{\text{now}}$ for most of the parameter space we consider (see Fig. 4 for an illustration).

In Fig. 4 we show the relationship between m_D and m_N obtained by numerically solving for

$$\langle m_\nu \rangle_{\text{now}} = \frac{\int d\chi m_D \lambda_-(\chi) [V_{\text{max}} - V(\chi)]^{-1/2}}{\int d\chi [V_{\text{max}} - V(\chi)]^{-1/2}} = 0.1 \text{ eV} , \quad (4.39)$$

over a period of oscillation, with λ_- given by Eq. (4.13).⁷ We find that the function

$$m_D = \frac{a}{(1 + (b \times m_N)^c)^{\frac{1}{2c}}} , \quad (4.40)$$

provides a good model for $m_D(m_N)$ when its parameters are fit to the numerical solutions. The parameters a , b , and c are then functions of g and m_ϕ . Notice, remarkably, that as m_N increases we always find that m_D must *decrease* in order to maintain $\langle m_{\nu,\text{now}} \rangle = 0.1 \text{ eV}$.

⁶Since the minimum is close to zero and the oscillations nearly harmonic after zero crossing, the 'typical' seesaw relationship holds, so we replace the m_D in Eq. (4.34) with $\sqrt{m_N m_\nu}$ in calculating this limit.

⁷In practice, we use the large- χ expansion of λ_- for the purposes of numerical stability.

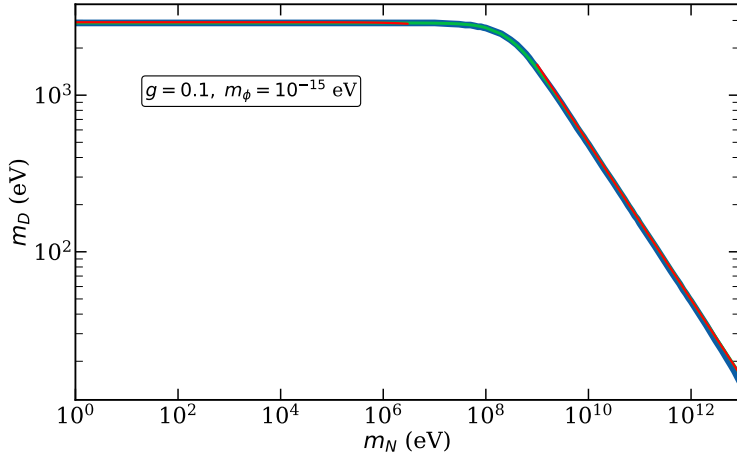


Figure 4: Modified seesaw relationship between m_D and m_N for initial conditions such that $\phi_0 > \phi_c$. The curve is defined by demanding $\langle m \rangle_\nu = 0.1$ eV today, and solving for m_D . The blue line is the numerical solution, while the green line is the approximation given in Eq. (4.40). For this value of g and m_ϕ , we find that the parameters are given by $a = 2.9 \times 10^3$ eV, $b = 3.4 \times 10^{-9}$ eV $^{-1}$, and $c = 1.4$. The red lines are given by $1.6 \times \frac{m_D^2}{g\varphi_{\min}}$ for small values of m_N and $4.7 \times \frac{m_D^2}{g\varphi_{\min}}$ for large values of m_N . We find that these are very good approximations to the numerical solution across different values of g and m_ϕ except along the ‘kink’ in the plots. The location of the kink scales inversely with m_ϕ , i.e. for this value of g it is given by approximately $10^8 \times \frac{10^{-15}}{m_\phi}$ eV. Notice that m_D actually *decreases* with increasing m_N .

4.4 Oscillations begin before neutrino decoupling

So far we have focused on $m_\phi \lesssim 10^{-14}$ eV such that neutrinos are decoupled relics throughout the entirety of the scalar fields’ oscillating dynamics. For $m_\phi \gtrsim 10^{-14}$ eV one has $T_{\text{osc}} \gtrsim T_{\nu,\text{dec}}$ and neutrinos are in thermal equilibrium at early times. Eventually, neutrinos will still decouple, and the cosmological epochs described above will follow similar dynamics. Therefore, the constraints derived by considering the cosmological epoch in which $T < T_{\text{dec}}$ apply to all cosmologies. Nevertheless, it is interesting to understand how the scalar field’s dynamics differs in a cosmological epoch where neutrinos are in thermal and chemical equilibrium.

We first begin by discussing the thermal potential, which assumes that neutrinos scatter with the rest of the Standard Model plasma quickly enough to remain in equilibrium. Then we discuss dynamical implications. At temperatures below a GeV (or so) we find that the neutrino interaction rate is not fast enough to keep neutrinos in thermal equilibrium on (very short) dynamical time scales that determine whether or not the field experiences zero crossings. This modifies the interpretation of certain cosmological constraints as we will see in Section 5.2. As we will argue in what follows, this inhibits zero-crossings of the field, and we do not expect any strong constraints from the epoch of BBN.

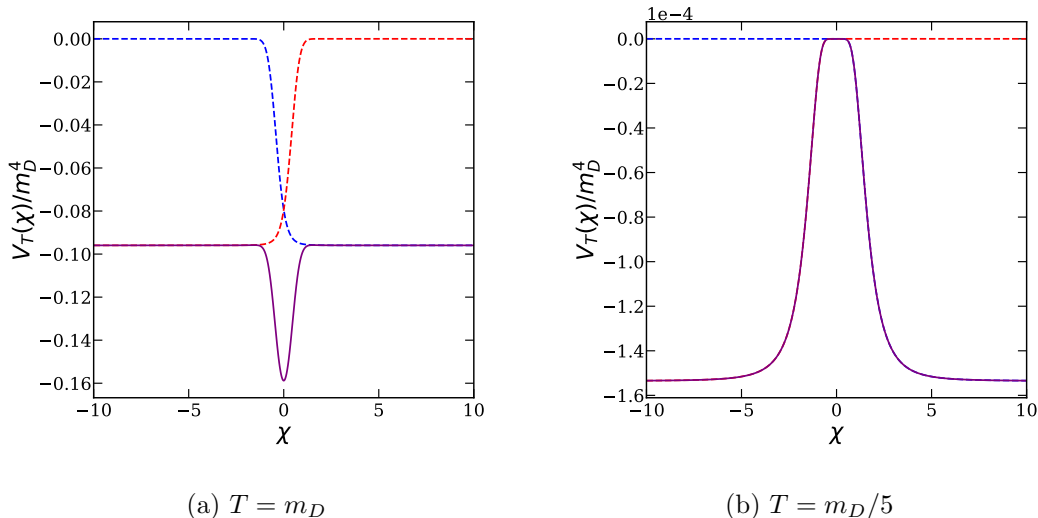


Figure 5: The thermal potentials $V_T(\chi)/m_D^4$, as given in Eq. (4.41), for ν_+ (red-dashed) and ν_- (blue-dashed) and their total sum (purple-solid) plotted for different values of T/m_D . **(a)** The potential has a minimum at $\chi = 0$ for $T \gtrsim 0.6m_D$ whereas **(b)** it has a barrier for $T \lesssim 0.6m_D$.

The thermal potential

If oscillations of the ϕ field start before neutrino decoupling, then the neutrino is still in the thermal bath. This leads to an additional contribution to the potential from the free energy of the light neutrino of the form [62]

$$V_{\text{thermal}}(\phi) = -\frac{T^4}{2\pi^2} J_F[m_L^2(\phi)/T^2], \quad (4.41)$$

where J_F is the fermionic thermal function (free energy density)

$$J_F(m_L^2/T^2) = \int_0^\infty dx x^2 \log\left(1 + e^{-\sqrt{x^2 + m_L^2/T^2}}\right). \quad (4.42)$$

Here $m_L = m_L(\phi)$ is the mass of the light neutrino species. For $T \gg m_L$ the thermal function has a simple high-temperature expansion,

$$J_F(m_L^2/T^2) \simeq \frac{\pi^2}{24} \frac{m_L^2}{T^2} + O(m_L^4/T^4). \quad (4.43)$$

We will assume that the number density of the heavy neutrino is Boltzmann suppressed i.e., that $m_H \gg T$.

Dynamical implications

When neutrinos are in thermal equilibrium, the relic potential introduced above is replaced by the thermal potential of Eq. (4.41). The thermal potential for χ stems from the free energy of the neutrino gas (in thermal and chemical equilibrium) as a function of neutrino

mass. Since m_L and m_H are functions of ϕ , the thermal functions for both the light- and heavy-species are implicit functions of ϕ , and serve as effective potentials which control the scalar field's dynamics. For simplicity, we will specialize to initial conditions such that $\phi_0 < \phi_c$, however our qualitative conclusions apply to both initial conditions to the left and right of ϕ_c .

As shown in Fig. 5, depending on the ratio of m_D/T the combined thermal potential for ν_+ and ν_- can have a minimum or maximum at $\chi = 0$. The reliability of the potential, however, depends on whether or not neutrinos have enough time to thermalize. The typical period of an oscillation cycle is set by $\tau_\phi \sim 1/m_\phi$ involving an oscillation amplitude of order χ_L (or χ_R when considering initial conditions where $\phi_0 > \phi_c$). The sharp features in Fig. 5 only occur over a region of $\Delta\chi \sim O(1)$. In order for the neutrinos to maintain thermal equilibrium during this small window, they must scatter efficiently over a time scale given by $\Delta\tau \sim (\Delta\chi/\chi_L) \times \tau_\phi$. This is a much shorter time scale than τ_ϕ .

Setting the neutrino interaction time-scale, $\tau_\nu \sim 1/(G_F^2 T^5)$ where $G_F = 1.116 \times 10^{-5} \text{GeV}^{-2}$ is the Fermi-constant, equal to the relevant time scale $\Delta\tau \sim \tau_\phi/\chi_L$, we find the temperature at which equilibrium can be maintained dynamically

$$T_{\text{dyn-eq}} \sim 100 \text{ GeV} \left(\frac{g}{0.1} \right)^{2/7} \left(\frac{1 \text{ MeV}}{m_D} \right)^{2/7}. \quad (4.44)$$

For $T \lesssim T_{\text{dyn-eq}}$ the thermal potential is a bad approximation near $\chi = 0$. Instead it is more appropriate to use the relic potential at these temperatures, because the (suddenly) heavy neutrinos do not have enough time to adjust their phase space distribution via scattering and decays. The analysis of Section 4.2 therefore applies immediately for $T \lesssim T_{\text{dyn-eq}}$, and we expect no zero crossings.

Since $T_{\text{dyn-eq}} \gg T_{\text{BBN}}$ we expect any effects due to the thermal potential (e.g., spectral distortions or decays $\nu_H \rightarrow \nu_L \phi$) to occur at early epochs and to be diluted by cosmic expansion. Furthermore, since $T_{\text{dyn-eq}}$ depends weakly on both g and m_D , we do not expect any interesting constraints from the epoch of BBN (e.g., the helium to deuterium abundance ratio Y_p) for any of the parameter space we consider.

5 Phenomenology

In this section we discuss a number of different constraints that arise both from laboratory experiments and cosmological considerations. The constraints are summarized in Section 5.5 in Figs. 7 and 8 (see also Eq. (5.19) which is not plotted).

5.1 Neutrino oscillation experiments

The time evolution of cosmic fields, such as our ultralight scalar dark matter candidate, can distort measurements of neutrino oscillation parameters. When τ_ϕ is very long, explicitly time varying effects (such as periodicities in the solar neutrino flux) can be searched for using solar neutrinos [33]. If the period of oscillation, $\tau_\phi = 2\pi/m_\phi$, is large relative to neutrino time of flight, $t_{\nu,\text{tof}}$, but small compared to the run-time of an experiment, DiNO signals are observable. For the smallest values of τ_ϕ (or the largest values of m_ϕ), oscillations

are too fast and DiNO signals cannot probe these regions of parameter space ($m_\phi \gtrsim 10^{-11}$ eV).

We follow [17] and set constraints at constant η_ϕ , as defined using the explicit model given by Eq. (1.2), as

$$\eta_\phi \equiv \frac{\delta m_L}{m_L}, \quad (5.1)$$

For Fig. 7 we set a constraint at $\eta_\phi \lesssim 0.032$ from the KamLAND constraint of [17], which is the most restrictive DiNO constraint for $m_\phi \lesssim 10^{-11}$ eV, and $\eta_\phi \lesssim 0.21$ for 10^{-11} eV $\lesssim m_\phi \lesssim 10^{-9}$ eV from the Daya Bay constraint. For $T_{\text{drop}} > T_{\text{now}}$, where the brief period of anharmonicity in oscillations to the left of ϕ_c has ended, we have relaxed to approximately harmonic oscillations about the minimum of the bare potential (see Fig. 2c). Therefore in this regime, $\eta_\phi = g\sqrt{2\rho_{\text{DM,now}}^\oplus}/(m_\phi m_N)$ is used to calculate the constraint on m_N (just like in [17]) where $\rho_{\text{DM,now}}^\oplus$ is the local density of dark matter, 2×10^{-6} eV. Below this line, the ‘drop’ has not yet occurred today and the oscillations of the scalar field are very large (see Fig. 2a). As such, we expect neutrino parameters, such as the mass, to vary substantially (i.e., with an $O(1)$ oscillation amplitude) in time and be constrained by DiNO measurements for $m_\phi \lesssim 10^{-9}$ eV for Daya Bay, and $m_\phi \lesssim 10^{-11}$ eV for KamLAND [17, 18].

For Fig. 8 the correct interpretation of the constraints on η_ϕ is more subtle. Unlike in Refs. [17, 18], we do not assume sinusoidal oscillations about the potential’s minimum, nor do we assume the standard see-saw relationship between m_N and m_D . Instead m_D is related to m_N via the modified seesaw relationship approximated by Eq. (4.40). Based on Eq. (5.1), as a rough proxy for these experimental constraints we calculate

$$\eta_\phi \sim \frac{\mu_-(\varphi_L) - \mu_-(\varphi_R)}{m_{\nu,\text{now}}} = \frac{\mu_-(\varphi_L) - \mu_-(\varphi_R)}{0.1 \text{ eV}}, \quad (5.2)$$

with μ_- given by Eq. (2.5). The left and right turning points, $\varphi_{L/R}$ (or equivalently, $\chi_{L/R}$), are determined by numerically solving Eq. (4.31) and using Eq. (4.40) to determine m_D for a given m_N , m_ϕ , and g . We find that this approximation for η_ϕ is consistently around 80 - 90 for $T_{\text{cross}} < T_{\text{now}}$, which therefore rules this region of parameter space out (the rest of parameter space being mostly ruled out by overclosure, see Fig. 8).

To perform the full analysis for Fig. 7 would require a similar determination of the modified seesaw relationship in the parameter space where T_{drop} has not yet occurred and oscillations are asymmetric. One could then follow a similar procedure as described above to calculate Eq. (5.1) and estimate if this region of parameter space is ruled-out by DiNO experiments. A complete analysis would compute $m_L(t)$ properly solving the equations of motion, but this lies beyond the scope of this paper.

5.2 Neutrino mass and the CMB

As mentioned in the introduction, previous studies of ULDM coupled to neutrinos have inferred a bound from the cosmic neutrino background. This is obtained by demanding $\langle m_\nu \rangle_{\text{RMS}} \lesssim 0.1$ eV at CMB where the right-hand side coming from published constraints

from the Planck collaboration.⁸ In [17] this translates into a constraint on $\eta_\phi > (9 \times 10^{-3}$ or 0.1) being excluded (depending on whether couplings to lighter or heavier active neutrinos are considered). As we will now argue, this constraint can be substantially modified once the relic potential is incorporated.

Scenarios where naive constraints applies

Let us begin by discussing which scenarios map onto the analysis in [17] most closely. When Eq. (4.3) is satisfied, the relic potential is not important at the CMB. This allows the naive constraint, where the field is redshifted with the typical $\rho \propto (T_{\text{now}}/T)^3$ scaling, to apply immediately. Notice, however, that the parameter space where Eq. (4.3) applies gives $\eta_\phi \ll 10^{-3}$ and so the CMB constraint on the neutrino mass is not informative. We therefore conclude that the CMB never supplies an interesting constraint on the model in the regions where the neutrino background density can be ignored for all $T < T_{\text{osc}}$.

Large negative initial conditions

Next, consider oscillations that begin to the left of ϕ_c . If $T_{\text{drop}} \gg T_{\text{CMB}}$ then the oscillations are predominantly about ϕ_{min} , and therefore well separated from ϕ_c ; in this case the analysis of [17] again apply immediately.

If $T_{\text{drop}} \lesssim T_{\text{CMB}}$, then the amplitude of oscillations at the epoch of the CMB is large. The light neutrinos, ν_L , spend part of their time with $|\chi| \sim O(1)$ which leads “large” masses, $m_L \sim m_D$, on the order of the Dirac mass. The time in which $m_L \sim m_D$ is short, being suppressed by $\Delta\tau/\tau_\phi \sim 1/|\chi_L|$, where $\Delta\tau$ is the time spent near the turning point and τ_ϕ is the period of oscillation. Therefore we will consider parameter space such that

$$T_{\text{now}} \lesssim T_{\text{drop}} \lesssim T_{\text{CMB}} , \quad (5.3)$$

corresponding to the green band in Fig. 7. By focusing on regions where $T_{\text{now}} < T_{\text{drop}}$ we are able to use the typical see-saw relationship to relate m_D and m_N . With these assumptions, in order for the mass of neutrinos to be sufficiently small at the epoch of the CMB, we require $m_D/\chi_L \lesssim 0.1$ eV, or equivalently (using $\chi_L \simeq g\phi_L/(2m_D)$),

$$\frac{2m_D^2 m_\phi}{g\sqrt{2\rho_{\text{DM,now}}}} \left(\frac{1}{1100}\right)^{3/2} \lesssim 0.1 \text{ eV} , \quad (5.4)$$

to avoid constraints from the CMB, where we use $m_\nu \lesssim 0.1$ eV as a rough proxy for the constraint on the sum of neutrino masses.

We find that Eq. (5.4) is a reasonable approximation to the numerical solution (obtained by solving Eq. (3.1) for a period of oscillation, neglecting Hubble friction), but typically overestimates the time-averaged neutrino mass by a factor of ~ 2 . When calculating the numerical solution we solve, $\ddot{\chi} = -\frac{dV}{d\chi}$, with $V(\chi)$ given by Eq. (4.12) where we take $T \ll m_D\lambda_+$ at T_{CMB} .⁹ We then use the Taylor-expansion of $m_D\lambda_+$ for large $|\chi|$

⁸The constraint is on the sum of neutrino masses but since we work in a simplified 1 + 1 framework this is irrelevant for our present discussion.

⁹In practice, when calculating the mass we use the large- $|\chi|$ expansion of $m_D\lambda_+$ for the purposes of numerical stability.

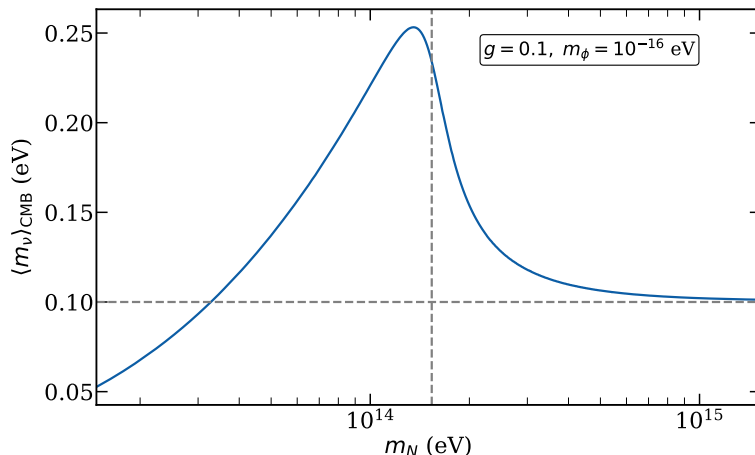


Figure 6: Time-averaged neutrino mass at the epoch of the CMB, $\langle m_\nu \rangle_{\text{CMB}}$ as a function of m_N , for initial conditions to the left. We have used $g = 0.1$ and $m_\phi = 10^{-16}$ eV as illustrative parameters. The vertical dashed gray line represents the value of m_N for which $T_{\text{drop}} = T_{\text{CMB}}$, while the horizontal dashed gray line represents $\langle m_\nu \rangle_{\text{now}}$. Notice that for sufficiently high m_N , $\langle m_\nu \rangle_{\text{CMB}}$ asymptotically approaches $\langle m_\nu \rangle_{\text{now}}$.

with λ_+ given by Eq. (4.13) to determine the time-average of the mass over the oscillation period, which we demand is less than 0.1 eV. This gives us an upper bound on m_D in terms of m_ϕ .

Translating Eq. (5.4) from m_D to m_N using the seesaw relationship (that applies today) $m_{\nu, \text{now}} = 0.1 \text{ eV} = m_D^2/m_N$, we obtain a bound on m_N above which neutrinos are too heavy at the epoch of the CMB (blue region in Fig. 7). However, for sufficiently high m_N , the constraint no longer applies. This can be understood in the context of Fig. 2c. After the “drop”, the potential takes the approximate shape of a simple harmonic oscillator with minimum given by (negative) Eq. (4.11). The minimum moves further away from $\varphi = 0$ in Fig. 1 for increasing m_N which tends to decrease the value of $\langle m_\nu \rangle_{\text{CMB}}$. Eventually, the minimum becomes so well-separated from the relic potential wall that we can neglect its contribution entirely and treat the potential as just the bare, harmonic potential. In this regime, the time-average of the mass-oscillations are well-approximated by their value at the minimum, which necessarily matches m_ν today.

This behavior is shown in Fig. 6, where one can clearly see the crossover between the two different regimes. The cross over occurs at m_N such that $T_{\text{drop}}(m_N) \simeq T_{\text{CMB}}$ (obtained by solving Eq. (4.22)). As m_N tends to larger values the average neutrino mass at T_{CMB} becomes equal to its value now, which we have fixed to be 0.1 eV.

Large positive initial conditions

Next we consider the case of oscillations to the right of ϕ_c with $T_{\text{cross}} < T_{\text{now}}$ such that zero crossings have never occurred. In this regime the minimum of the potential tends closer to the steep relic potential wall at $\chi = 0$ in Fig. 3a as the temperature decreases (see

Eqs. (4.27) and (4.28)). This means that the average neutrino mass tends to increase with decreasing temperature. Therefore we are guaranteed that if neutrinos are 0.1 eV today, then they were lighter than 0.1 eV at the CMB and no constraint exists. For $T_{\text{cross}} > T_{\text{now}}$ the parameter space is mostly ruled out by overclosure and so we do not consider this regime here (see Fig. 8).

5.3 Supernova cooling

Constraints from supernova cooling were analyzed in Ref. [17]. The assumed energy loss channel was $\nu_L \bar{\nu}_L \rightarrow \phi\phi$ with a cross section given parametrically by

$$\sigma \sim \frac{g^4}{T^2} \left(\frac{m_L}{m_H} \right)^4. \quad (5.5)$$

This scaling stems from the need to insert two mixing angles $\theta_L^2 \sim (m_L/m_H)$ in the leading Feynman diagram; the temperature scaling arises from naive dimensional analysis.

In the interior of a supernova the density of neutrinos is very large (just like in the early universe). An immediate consequence is that mostly-active neutrinos are much lighter in a supernova than in vacuum $m_{L,\text{SN}} \ll m_{L,\text{vac}}$, while mostly-sterile ones are much heavier $m_{H,\text{SN}} \gg m_{H,\text{vac}}$. For $T_{\text{SN}} \sim 30$ MeV this suppresses the cross section for $\nu\bar{\nu} \rightarrow \phi\phi$ by orders of magnitude and essentially eliminates the supernova cooling constraint considered in Ref. [17].

Light neutrinos can also annihilate via an off-shell heavy neutrino with a cross section that scales, for $T \ll m_H$, as

$$\sigma \sim \frac{g^4}{m_H^2} \left(\frac{m_L}{m_H} \right)^2 \gg \frac{g^4}{T^2} \left(\frac{m_L}{m_H} \right)^4. \quad (5.6)$$

We therefore conclude that for any temperature satisfying $T \gg m_L$

\(\gg\)

We will follow the same parametric estimate sketched in Ref. [17], but using the $\nu^2\phi^2$ (that arises from integrating out ν_H) vertex rather than the $\nu^2\phi$ vertex. Taking the rate of energy loss per neutrino per unit time to be $\dot{E}_\nu \sim T_{\text{SN}} n \sigma$, and a thermal density of $n_\nu \sim 9\zeta(3)T_{\text{SN}}^3/(4\pi)^2$, we find

$$\dot{E}_\nu \sim 5 \times 10^{-4} \frac{\text{erg}}{s} \left(\frac{T_{\text{SN}}}{30 \text{ MeV}} \right)^4 \left(\frac{1 \text{ GeV}}{m_H} \right)^4 \left(\frac{m_L(T_{\text{SN}})}{0.1 \text{ eV}} \right)^2 \left(\frac{g}{0.1} \right)^4. \quad (5.7)$$

For $\sim 4 \times 10^{54}$ neutrinos in a supernova, we require $\dot{E}_\nu \lesssim 10^{-5} \text{erg/s}$. Since $m_L(T \sim 30 \text{ MeV}) \ll m_{\nu, \text{now}}$ and m_H is generically much larger than m_N , we expect that supernova

bounds are essentially always satisfied. We therefore do not include them in our summary plots Figs. 7 and 8.

5.4 Cosmologically stable condensate

In order for the misaligned scalar condensate to survive at late times we require that particles in the bath do not destroy the condensate. In particular the scattering of neutrinos from the condensate $\nu\phi \rightarrow \nu\phi$ should have a rate smaller than Hubble H [63].

As discussed in Eq. (5.6), the largest scattering rate (per ϕ particle) is mediated by an off-shell heavy neutrino. A conservative requirement is that this rate is small compared to Hubble at all cosmic epochs after reheating. In what follows we will assume that $T_{\text{RH}} \gtrsim 10$ MeV (slightly larger than the estimated minimum temperature of 4 MeV).

The rate per scalar particle (in the $m_L \ll m_H$ limit) scales as

$$\Gamma \sim \frac{g^2 T^3}{(4\pi)m_H^2} \theta_L^4, \quad (5.8)$$

The scaling of $m_L(T)$ and $m_H(T)$ with temperature depend on the initial conditions. For initial condition that begin at large negative field values, the mixing angle is maximized at the right turning point $\chi = \chi_R$ (the closest point of approach to a Dirac pair).

Oscillations begin after $T_{\nu,\text{dec}}$

For simplicity we will focus on the case of large negative initial conditions for the field ϕ . The mixing angle suppression of the $\nu\phi \rightarrow \nu\phi$ cross section, $\sin^4\theta$, is time-dependent. The cross section is largest close to the right-turning point ϕ_R given in Eq. (4.6). When written in terms of χ we have

$$\chi_R = - \left(\frac{m_D n_\nu(T)}{2\rho_\phi(T)} \right). \quad (5.9)$$

For $m_D \gtrsim 100m_\nu$, $n_{\text{now}} \simeq 10$ eV, $|\chi_R| \gg 1$ and we have

$$\sin^2\theta \simeq \frac{1}{4\chi^2}, \quad (5.10)$$

such that (also using the large χ approximation for m_H)

$$\Gamma \sim \frac{g^2 T^3}{(4\pi)m_D^2} \frac{1}{\chi^8}. \quad (5.11)$$

Since χ_R is independent of temperature until $T \sim T_{\text{drop}}$, and the rate is proportional to T^3 , this rate is maximized at the highest available temperature.

When integrated over an oscillation cycle, the time average is dominated by $\chi \simeq \chi_R$. We find that the rate, averaged over one oscillation cycle, is given by

$$\Gamma \sim \frac{g^2 T^3}{(4\pi)m_D^2} \frac{1}{\chi_R^8 \chi_L}. \quad (5.12)$$

Notice that $\chi_L \propto T^{3/2}$ and therefore $\chi_L \gg 1$. Furthermore, even for modest value of χ_R (e.g., $\chi_R \sim 100$) the suppression from $1/\chi_R^8$ is extremely large.

If the field has not yet started oscillating, then χ is stuck at χ_L and we find a rate that is suppressed by $1/\chi_L^8$. We therefore take the largest possible temperature as $T_{\text{osc}} \sim \sqrt{M_{\text{Pl}} m_\phi}$. Demanding $\Gamma \lesssim H \sim T^2/M_{\text{Pl}}$ requires,

$$\frac{g^2}{\chi_R^8 \chi_L} \ll \frac{m_D^2}{T_{\text{osc}} M_{\text{Pl}}} . \quad (5.13)$$

This condition is easily satisfied even for $g \sim O(1)$. We therefore do not include constraints from a ruptured condensate for $m_\phi \leq 10^{-14}$ eV in what follows.

Oscillations begin before $T_{\nu, \text{dec}}$

For larger masses $m_\phi \geq 10^{-14}$ eV, the field will oscillate prior to neutrino decoupling. If the field is able to cross $\chi = 0$, this can lead to short periods in which there are pseudo-Dirac pairs each coupling to ϕ with a strength of $g/\sqrt{2}$. The period of time spent near $\chi \sim O(1)$ is suppressed by the large oscillation amplitude χ_L , such that the time averaged mixing angle is

$$\langle \sin^2 \theta \rangle \sim \frac{1}{2\chi_L} . \quad (5.14)$$

Therefore, in this epoch, the rate averaged over an oscillation cycle is set by

$$\Gamma \sim 2 \times \frac{g^2 T^3}{(4\pi) m_D^2} \frac{1}{2\chi_L} = \frac{g m_\phi T^3}{(4\pi) m_D \sqrt{2\rho_{\text{DM}}}} , \quad (5.15)$$

where the pre-factor of 2 accounts for both ν_+ and ν_- during this epoch.

Using $\rho_\phi \approx 0.7 \text{ eV} \times T^3$ we find

$$\Gamma \sim \frac{g T^{3/2} m_\phi}{8\pi m_D \sqrt{1.4 \text{ eV}}} . \quad (5.16)$$

Notice that when measured in units of Hubble in a radiation dominated universe, $H \sim T^2/M_{\text{Pl}}$, the rate will be fastest at the *highest* temperatures. In order for the condensate not to rupture we therefore require that $\Gamma(T_{\text{osc}}) < H(T_{\text{osc}}) = m_\phi/3$, which leads to

$$\left(\frac{g^2 T_{\text{osc}}^2}{64\pi^2 m_D^2} \right) \left(\frac{T_{\text{osc}}}{1.4 \text{ eV}} \right) < \frac{1}{9} , \quad \text{or} \quad m_D \gtrsim 10 \text{ MeV} \left(\frac{T_{\text{osc}}}{1 \text{ MeV}} \right)^{3/2} \left(\frac{g}{0.1} \right) . \quad (5.17)$$

Alternatively, we can avoid rupturing the condensate if $m_D \gtrsim 0.6 \times T_{\text{osc}}$ such that there is a barrier (rather than minimum) near $\chi = 0$ as shown in Figs. 5a and 5b. Therefore, if g is larger than the bound in Eq. (5.17), but

$$m_D \geq 0.6 \times T_{\text{osc}} , \quad (5.18)$$

then the condensate does not rupture because the thermal potential does not allow the field to cross $\chi = 0$.

In summary, we expect that the condensate will survive provided

$$m_D \geq \min(\text{Eq. (5.17)} , \text{Eq. (5.18)}) . \quad (5.19)$$

For $T_{\text{drop}} > T_{\text{now}}$ this gives a lower-bound on m_N via $m_D = \sqrt{m_{\nu, \text{now}} m_N}$ which only applies to already-excluded parameter space in Fig. 7. For $T_{\text{drop}} < T_{\text{now}}$ we would need to determine the modified seesaw relationship to correctly incorporate the constraint of Eq. (5.19), which lies outside the scope of this paper.

5.5 Summary of constraints

For simplicity we organize our constraints according to initial conditions. Figure 7 shows constraints for initial conditions such that $\phi_0 < 0$ whereas Fig. 8 shows constraints for initial field values satisfying $\phi_0 > \phi_c$.

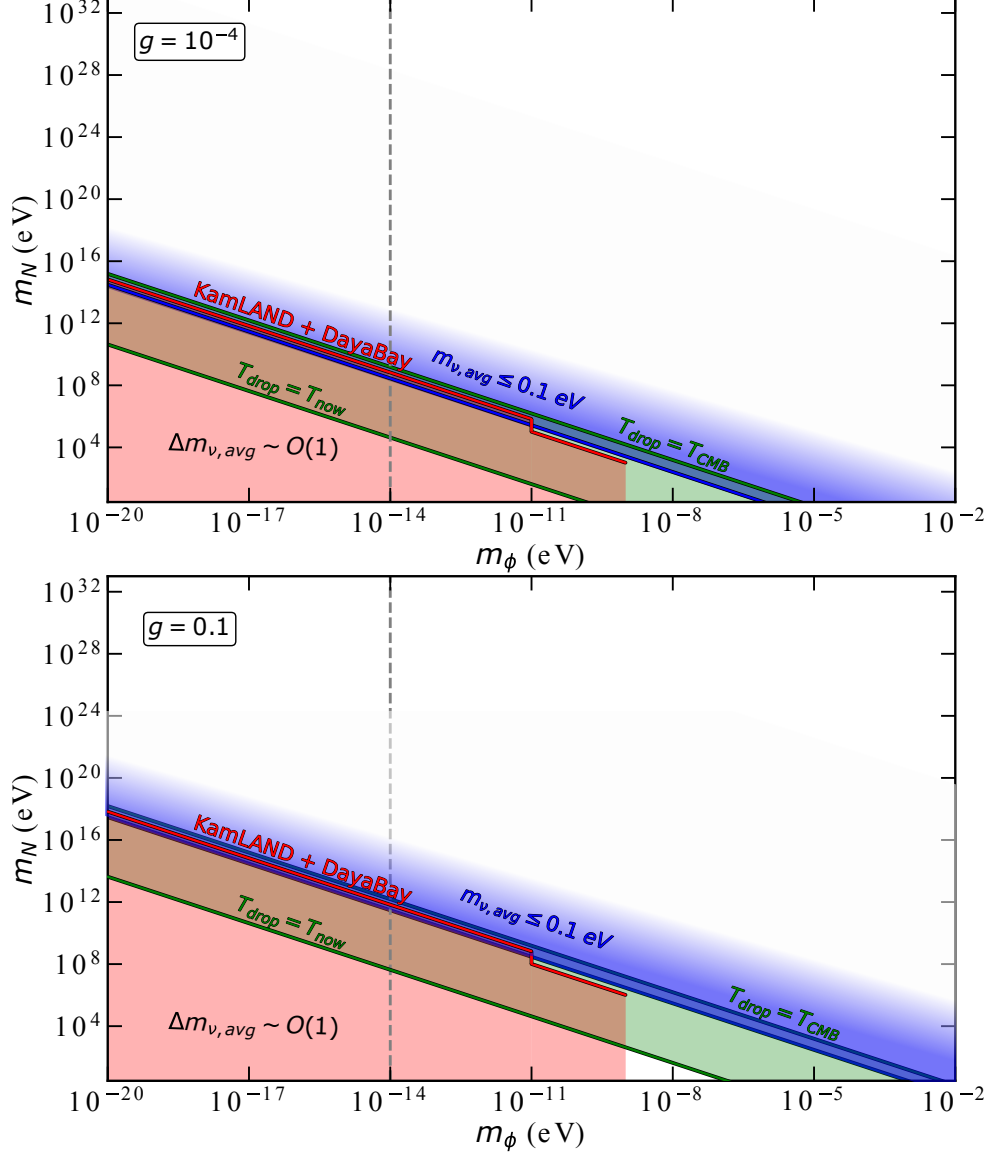


Figure 7: Parameter space for ϕ -induced variations in the neutrino mass for $\phi_0 < 0$. The gray dashed line marks $m_\phi = 10^{-14}$ eV above which $T_{\text{osc}} > T_{\nu, \text{dec}}$. The red-shaded region is ruled out by searches for DiNOs (Section 5.1). The blue region leads to unacceptably large time-averaged neutrino masses at T_{CMB} (Section 5.2); we shade with a gradient since this is a smooth cross-over as shown in Fig. 6. The green band denotes the region where there is a sudden “drop” in the dark matter energy density between the epoch of the CMB and now; this region is disfavoured (see Eq. (4.21)). Below the green band the scalar has a large oscillation amplitude today and we expect $O(1)$ time-variation of neutrino mass.

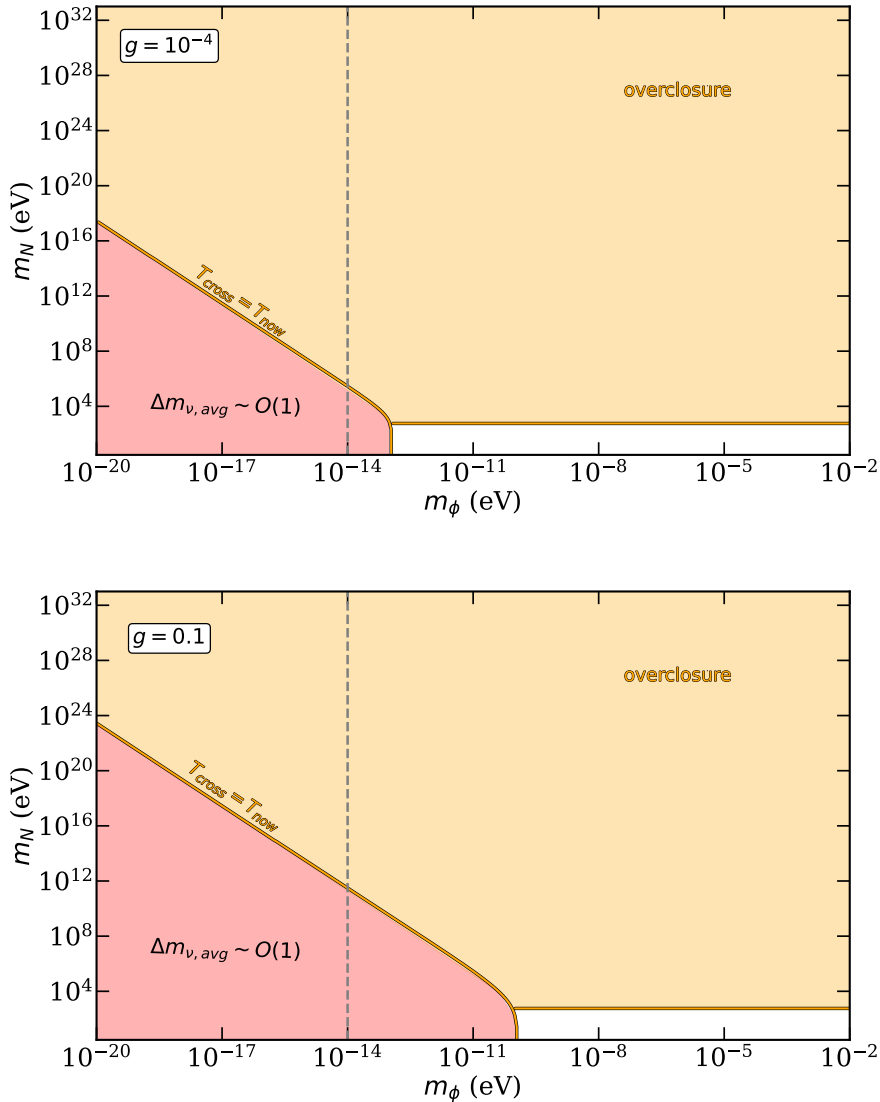


Figure 8: Parameter space for ϕ -induced variations in the neutrino mass for $\phi_0 > \phi_c$. The gray dashed line marks $m_\phi = 10^{-14}$ eV above which $T_{\text{osc}} > T_{\nu, \text{dec}}$. The red region is ruled out by searches for DiNOs (Section 5.1). In the yellow region the field is trapped at $\phi > \phi_c$ at early times, but eventually crosses ϕ_c and overcloses the universe (Section 4.3).

As can be seen by comparing Figs. 7 and 8, we find that the cosmology differs qualitatively depending on whether ϕ_0 is less than or greater than ϕ_c . In the former case, Fig. 7, neutrinos retain their adiabatic label throughout all of cosmic history. We find that constraints from $\langle m_\nu \rangle_{\text{CMB}}$ complement rather than compete with constraints from DiNOs. When $\phi_0 > \phi_c$, Fig. 8, the scalar field either crosses ϕ_c before today, or it has not yet crossed ϕ_c in which case it is oscillating in a shallow and highly asymmetric potential. The former option is ruled out because it would overclose the universe (unless $m_N \leq 600$ eV), while the latter scenario is ruled out by DiNOs.

6 Conclusions and outlook

The main results of this paper pertain to the cosmology of scalar fields coupled to multiple fermions. The eigenvalues of a simple model of a scalar coupled to right-handed neutrinos (plotted in Fig. 1) naturally generate a highly asymmetric potential for the scalar field as show in Figs. 2a, 2b and 3a. The contribution of this highly asymmetric potential grows with temperature and dominates the scalar field’s dynamics in the early universe.

Motivated by these general observations, we have studied a simple 1 + 1 model of sterile neutrinos. We find that the altered potential of the scalar can both modify its cosmology, but also its present day dynamics. We find the dynamics of the scalar field are dominated by the relic potential in many regions of parameter space. Furthermore, based on the analysis of our simplified 1 + 1 model, that viable parameter space requires scalar masses larger than $m_\phi > 10^{-9}$ eV, relatively large couplings $g \gtrsim 10^{-5}$, and initial conditions where $\phi_0 < \phi_c$. This region corresponds to the lower triangle in Fig. 7.

These conclusions have immediate applications to searches for time-varying or distorted neutrino oscillations (DiNOs) [17–25]. Furthermore, the temperature dependence of the relic potential, Eq. (3.6), can lead to a temporarily modified equation of state for the scalar field. A large fraction of the available parameter space in Fig. 7 is shaded green, implying that the dark matter relic density would have a modified equation of state at some time between $z = 1$ and $z \approx 1100$. We consider this region to be disfavored, but not ruled out, in the absence of a detailed analysis. The modification of the equation state could be constrained using cosmological simulation tools such as CLASS [64].

One possibility we have not fully explored is the role of the high-temperature relic potential when $m_D \lesssim T$. We are most interested in the possibility of zero-crossings, and so m_D dictates which approximation of V_{relic} in Eq. (3.6) is valid since the mass of the light neutrino approaches $m_L \sim m_D$ as the field approaches the zero-crossing point. The condition $m_D \gg T$, assumed in the main text, guarantees that the low-temperature limit of the relic potential is valid when computing the turning point closest to $\chi = 0$. As the temperature of the bath increases the coefficient of the relic potential changes from $\mu_\pm T^3$ to $\mu_\pm^2 T^2$ (see Eq. (3.6)). This change in behaviour can “soften” the potential barrier and allow relic neutrinos to undergo a transition from light to heavy states $\nu_L \rightarrow \nu_H$. Notice, in particular, that the energy density in the scalar field is proportional to T^3 and so at sufficiently high temperatures grows faster than $\mu_\pm T^2$. Whether or not this is cosmologically viable, and if any observational signatures exist, is an interesting question that could be studied further.

Another interesting extension of this work would be to study the role of the relic potential for pseudo-Dirac neutrinos. These models have non-trivial cosmologies and can be probed down to very weak couplings [23, 25]. The role of the relic potential would be qualitatively different in a pseudo-Dirac scenario since both eigenstates would be present in the early universe. The relic potential would become symmetric about $\chi = 0$, and there could be an interesting interplay between the scalar’s conservative dynamics in the potential, and its dissipative dynamics from $\nu_H \rightarrow \nu_L \phi$ decays.

In summary, we find that decoupled cosmic relics can substantially alter a scalar field’s dynamics whenever their mass depends¹⁰ on the scalar’s expectation value. This idea is well appreciated in the MaVNs literature, but seems less well studied in the context of ultralight dark mater (see [26, 65, 66] however for analogs involving the thermal potential). Any future search for distorted neutrino oscillations should carefully consider the present-day dynamics of the scalar field. Our work also provides a well motivated model for temperature dependent and asymmetric potentials. The temperature dependent and highly asymmetric potentials sourced by the massive cosmic relic can lead to a modified equation of state for ULDM and spoil concordance between cosmological observations from different epochs.

Acknowledgements

We thank Mark Wise for collaboration during early stages of this work. We thank Dave McKeen, Linda Xu, Kim Berghaus, Matheus Hostert, Saurunas Verner, Yohei Ema, and especially Gordan Krnjaic Akshay Ghalsasi and Nashwan Sabti for helpful discussions. We are grateful to Mark Wise, Pedro Machado, Clara Murgui, Akshay Ghalsasi, and Leonardo Badurina for feedback on early versions of this manuscript.

RP is supported by the Neutrino Theory Network under Award Number DEAC02-07CH11359. RP and ST are supported by the U.S. Department of Energy, Office of Science, Office of High Energy Physics under Award Number DE-SC0011632, and by the Walter Burke Institute for Theoretical Physics.

References

- [1] A. de Gouvêa, *Neutrino Mass Models*, *Ann. Rev. Nucl. Part. Sci.* **66** (2016) 197.
- [2] J. Cooley et al., *Report of the Topical Group on Particle Dark Matter for Snowmass 2021*, [2209.07426](#).
- [3] D. Antypas et al., *New Horizons: Scalar and Vector Ultralight Dark Matter*, [2203.14915](#).
- [4] E.G.M. Ferreira, *Ultra-light dark matter*, *Astron. Astrophys. Rev.* **29** (2021) 7 [[2005.03254](#)].
- [5] D.Y. Cheong, N.L. Rodd and L.-T. Wang, *A Quantum Description of Wave Dark Matter*, [2408.04696](#).
- [6] J. Preskill, M.B. Wise and F. Wilczek, *Cosmology of the Invisible Axion*, *Phys. Lett. B* **120** (1983) 127.
- [7] L.F. Abbott and P. Sikivie, *A Cosmological Bound on the Invisible Axion*, *Phys. Lett. B* **120** (1983) 133.
- [8] M. Dine and W. Fischler, *The Not So Harmless Axion*, *Phys. Lett. B* **120** (1983) 137.
- [9] M.S. Turner, *Coherent Scalar Field Oscillations in an Expanding Universe*, *Phys. Rev. D* **28** (1983) 1243.
- [10] R. Fardon, A.E. Nelson and N. Weiner, *Dark energy from mass varying neutrinos*, *JCAP* **10** (2004) 005 [[astro-ph/0309800](#)].

¹⁰It also would be interesting to understand if density-dependent potentials could alter the cosmology of derivatively coupled scalars.

- [11] A.W. Brookfield, C. van de Bruck, D.F. Mota and D. Tocchini-Valentini, *Cosmology of mass-varying neutrinos driven by quintessence: theory and observations*, *Phys. Rev. D* **73** (2006) 083515 [[astro-ph/0512367](#)].
- [12] D.B. Kaplan, A.E. Nelson and N. Weiner, *Neutrino oscillations as a probe of dark energy*, *Phys. Rev. Lett.* **93** (2004) 091801 [[hep-ph/0401099](#)].
- [13] N. Afshordi, M. Zaldarriaga and K. Kohri, *On the stability of dark energy with mass-varying neutrinos*, *Phys. Rev. D* **72** (2005) 065024 [[astro-ph/0506663](#)].
- [14] V. Barger, P. Huber and D. Marfatia, *Solar mass-varying neutrino oscillations*, *Phys. Rev. Lett.* **95** (2005) 211802 [[hep-ph/0502196](#)].
- [15] R. Fardon, A.E. Nelson and N. Weiner, *Supersymmetric theories of neutrino dark energy*, *JHEP* **03** (2006) 042 [[hep-ph/0507235](#)].
- [16] B.W. Lee and S. Weinberg, *Cosmological Lower Bound on Heavy Neutrino Masses*, *Phys. Rev. Lett.* **39** (1977) 165.
- [17] G. Krnjaic, P.A.N. Machado and L. Necib, *Distorted neutrino oscillations from time varying cosmic fields*, *Phys. Rev. D* **97** (2018) 075017 [[1705.06740](#)].
- [18] V. Brdar, J. Kopp, J. Liu, P. Prass and X.-P. Wang, *Fuzzy dark matter and nonstandard neutrino interactions*, *Phys. Rev. D* **97** (2018) 043001 [[1705.09455](#)].
- [19] A. Berlin, *Neutrino Oscillations as a Probe of Light Scalar Dark Matter*, *Phys. Rev. Lett.* **117** (2016) 231801 [[1608.01307](#)].
- [20] G.-y. Huang, M. Lindner, P. Martínez-Miravé and M. Sen, *Cosmology-friendly time-varying neutrino masses via the sterile neutrino portal*, *Phys. Rev. D* **106** (2022) 033004 [[2205.08431](#)].
- [21] K. Whisnant, J. Liao and D. Marfatia, *Light scalar dark matter at neutrino oscillation experiments*, *PoS NuFACT2018* (2018) 152.
- [22] G.-Y. Huang and N. Nath, *Neutrinophilic Axion-Like Dark Matter*, *Eur. Phys. J. C* **78** (2018) 922 [[1809.01111](#)].
- [23] A. Dev, P.A.N. Machado and P. Martínez-Miravé, *Signatures of ultralight dark matter in neutrino oscillation experiments*, *JHEP* **01** (2021) 094 [[2007.03590](#)].
- [24] M. Losada, Y. Nir, G. Perez and Y. Shpilman, *Probing scalar dark matter oscillations with neutrino oscillations*, *JHEP* **04** (2022) 030 [[2107.10865](#)].
- [25] A. Dev, G. Krnjaic, P. Machado and H. Ramani, *Constraining feeble neutrino interactions with ultralight dark matter*, *Phys. Rev. D* **107** (2023) 035006 [[2205.06821](#)].
- [26] C. Murgui and R. Plestid, *Coleman-Weinberg dynamics of ultralight scalar dark matter and GeV-scale right-handed neutrinos*, [2306.13799](#).
- [27] M. Blennow, E. Fernandez-Martinez, A. Olivares-Del Campo, S. Pascoli, S. Rosauero-Alcaraz and A.V. Titov, *Neutrino Portals to Dark Matter*, *Eur. Phys. J. C* **79** (2019) 555 [[1903.00006](#)].
- [28] B. Barman, P.S. Bhupal Dev and A. Ghoshal, *Probing freeze-in dark matter via heavy neutrino portal*, *Phys. Rev. D* **108** (2023) 035037 [[2210.07739](#)].
- [29] Y. Farzan and E. Ma, *Dirac neutrino mass generation from dark matter*, *Phys. Rev. D* **86** (2012) 033007 [[1204.4890](#)].

- [30] A. Ghalsasi, D. McKeen and A.E. Nelson, *Probing nonstandard neutrino cosmology with terrestrial neutrino experiments*, *Phys. Rev. D* **95** (2017) 115039 [[1609.06326](#)].
- [31] E. Ma, *Common origin of neutrino mass, dark matter, and baryogenesis*, *Mod. Phys. Lett. A* **21** (2006) 1777 [[hep-ph/0605180](#)].
- [32] E. Ma, *Verifiable radiative seesaw mechanism of neutrino mass and dark matter*, *Phys. Rev. D* **73** (2006) 077301 [[hep-ph/0601225](#)].
- [33] A. Berlin and D. Hooper, *Axion-Assisted Production of Sterile Neutrino Dark Matter*, *Phys. Rev. D* **95** (2017) 075017 [[1610.03849](#)].
- [34] F. Capozzi, I.M. Shoemaker and L. Vecchi, *Neutrino Oscillations in Dark Backgrounds*, *JCAP* **07** (2018) 004 [[1804.05117](#)].
- [35] M.M. Reynoso and O.A. Sampayo, *Propagation of high-energy neutrinos in a background of ultralight scalar dark matter*, *Astropart. Phys.* **82** (2016) 10 [[1605.09671](#)].
- [36] J.M. Cline, *Viable secret neutrino interactions with ultralight dark matter*, *Phys. Lett. B* **802** (2020) 135182 [[1908.02278](#)].
- [37] K.-Y. Choi, J. Kim and C. Rott, *Constraining dark matter-neutrino interactions with IceCube-170922A*, *Phys. Rev. D* **99** (2019) 083018 [[1903.03302](#)].
- [38] G.-y. Huang and N. Nath, *Neutrino meets ultralight dark matter: $0\nu\beta\beta$ decay and cosmology*, *JCAP* **05** (2022) 034 [[2111.08732](#)].
- [39] S. Pandey, S. Karmakar and S. Rakshit, *Interactions of astrophysical neutrinos with dark matter: a model building perspective*, *JHEP* **01** (2019) 095 [[1810.04203](#)].
- [40] E.J. Chun, *Neutrino Transition in Dark Matter*, [2112.05057](#).
- [41] K.-Y. Choi, E.J. Chun and J. Kim, *Neutrino Oscillations in Dark Matter*, *Phys. Dark Univ.* **30** (2020) 100606 [[1909.10478](#)].
- [42] M.M. Reynoso, O.A. Sampayo and A.M. Carulli, *Neutrino interactions with ultralight axion-like dark matter*, *Eur. Phys. J. C* **82** (2022) 274 [[2203.11642](#)].
- [43] Y. Farzan and S. Palomares-Ruiz, *Flavor of cosmic neutrinos preserved by ultralight dark matter*, *Phys. Rev. D* **99** (2019) 051702 [[1810.00892](#)].
- [44] Y. Farzan, *Ultra-light scalar saving the $3 + 1$ neutrino scheme from the cosmological bounds*, *Phys. Lett. B* **797** (2019) 134911 [[1907.04271](#)].
- [45] S.-F. Ge and H. Murayama, *Apparent CPT Violation in Neutrino Oscillation from Dark Non-Standard Interactions*, [1904.02518](#).
- [46] Y. Zhao, *Cosmology and time dependent parameters induced by a misaligned light scalar*, *Phys. Rev. D* **95** (2017) 115002 [[1701.02735](#)].
- [47] H. Davoudiasl and P.B. Denton, *Sterile neutrino shape shifting caused by dark matter*, *Phys. Rev. D* **108** (2023) 035013 [[2301.09651](#)].
- [48] M. Carrillo González, Q. Liang, J. Sakstein and M. Trodden, *Neutrino-Assisted Early Dark Energy: Theory and Cosmology*, *JCAP* **04** (2021) 063 [[2011.09895](#)].
- [49] P. Martínez-Miravé, Y.F. Perez-Gonzalez and M. Sen, *Effects of neutrino-ultralight dark matter interaction on the cosmic neutrino background*, *Phys. Rev. D* **110** (2024) 055005 [[2406.01682](#)].

- [50] Y. ChoeJo, Y. Kim and H.-S. Lee, *Dirac-Majorana neutrino type oscillation induced by a wave dark matter*, *Phys. Rev. D* **108** (2023) 095028 [[2305.16900](#)].
- [51] F. Goertz, M. Hager, G. Laverda and J. Rubio, *Phasing out of Darkness: From Sterile Neutrino Dark Matter to Neutrino Masses via Time-Dependent Mixing*, [2407.04778](#).
- [52] J. Sakstein and M. Trodden, *Early Dark Energy from Massive Neutrinos as a Natural Resolution of the Hubble Tension*, *Phys. Rev. Lett.* **124** (2020) 161301 [[1911.11760](#)].
- [53] M. Weber and W. de Boer, *Determination of the local dark matter density in our galaxy*, *Astronomy and Astrophysics* **509** (2010) A25.
- [54] PLANCK collaboration, *Planck 2018 results. VI. Cosmological parameters*, *Astron. Astrophys.* **641** (2020) A6 [[1807.06209](#)].
- [55] C. Zener, *Nonadiabatic crossing of energy levels*, *Proc. Roy. Soc. Lond. A* **137** (1932) 696.
- [56] S.J. Parke, *Nonadiabatic Level Crossing in Resonant Neutrino Oscillations*, *Phys. Rev. Lett.* **57** (1986) 1275 [[2212.06978](#)].
- [57] L.F. Abbott, E. Farhi and M.B. Wise, *Particle Production in the New Inflationary Cosmology*, *Phys. Lett. B* **117** (1982) 29.
- [58] P.B. Greene and L. Kofman, *Preheating of fermions*, *Phys. Lett. B* **448** (1999) 6 [[hep-ph/9807339](#)].
- [59] P.B. Greene and L. Kofman, *On the theory of fermionic preheating*, *Phys. Rev. D* **62** (2000) 123516 [[hep-ph/0003018](#)].
- [60] P. Adshead and E.I. Sfakianakis, *Fermion production during and after axion inflation*, *JCAP* **11** (2015) 021 [[1508.00891](#)].
- [61] A. Ghalsasi and A.E. Nelson, *Effects of Mass Varying Neutrinos on Cosmological Parameters as determined from the Cosmic Microwave Background*, *Phys. Rev. D* **90** (2014) 045002 [[1405.0711](#)].
- [62] M. Quiros, *Finite temperature field theory and phase transitions*, in *ICTP Summer School in High-Energy Physics and Cosmology*, pp. 187–259, 1, 1999 [[hep-ph/9901312](#)].
- [63] I. Dymnikova and M. Khlopov, *Decay of cosmological constant as Bose condensate evaporation*, *Mod. Phys. Lett. A* **15** (2000) 2305 [[astro-ph/0102094](#)].
- [64] J. Lesgourgues, *The cosmic linear anisotropy solving system (class) i: Overview*, 2011.
- [65] B. Batell and A. Ghalsasi, *Thermal misalignment of scalar dark matter*, *Phys. Rev. D* **107** (2023) L091701 [[2109.04476](#)].
- [66] B. Batell, A. Ghalsasi and M. Rai, *Dynamics of dark matter misalignment through the Higgs portal*, *JHEP* **01** (2024) 038 [[2211.09132](#)].